universität wien

MASTERARBEIT / MASTER'S THESIS

Titel der Masterarbeit / Title of the Master's Thesis

„Influence of Dietary Fatty Acids on Mechanosensory Apparatus on Intestinal Cell Lines"

verfasst von / submitted by

Janice Bergen BSc

angestrebter akademischer Grad / in partial fulfilment of the requirements for the degree of

Master of Science (MSc)

Wien, 2022/ Vienna, 2022

Studienkennzahl lt. Studienblatt / degree programme code as it appears on the student record sheet:	UA 066 659
Studienrichtung lt. Studienblatt / degree programme as it appears on the student record sheet:	Masterstudium Lebensmittelchemie UG 2002
	Ass.-Prof. Dott. ric. Giorgia Del Favero, Privatdoz.

Abstract

Mechanotransduction is the conversion of mechanical stimuli into biological signals. All living organisms are affected by mechanical forces in their environment, which ultimately contribute to survival through the sensory systems. Starting from the idea that our body can adapt to diet and lifestyle we started to investigate if exposure to fatty acids can tune the physiology of intestinal cells and in particular mechanotransduction. Analysing systematically the mechanosensory apparatus of the cells, we postulated an involvement of several elements: Firstly, Piezo1 channels, which are mechano-gated large Ca^{2+}-permeable non-selective cation channels. Recent findings suggest that Piezo channels play a role in pathophysiological processes including gut inflammation, cancers and cardiovascular mechanobiology. Moreover, Yes-associated protein 1 (YAP1) is a co-transcription factor in a number of biochemical pathways which regulate organ size, regeneration, and tumorigenesis. Furthermore, YAP1 is a potent oncogene in some cancers and therefore a potential target in the treatment of cancer. Both Piezo1 and YAP1 depend on mechanical cues for their functioning. Since palmitic acid (PA) and oleic acid (OA) are among the most prevalent fatty acids in the uptake of food and likewise the lipids building blocks which are known to alter mechanical properties of the membrane, the hypothesis is whether these fatty acids could lead to a modification of cell membrane fluidity, a difference in the distribution of Piezo1 channels, a change in the actin cytoskeleton or a variation of the translocation efficiency of YAP1. Experiments using a human colon cancer cell line (HCT 116) as well as a human immortalized epithelial colon cell line (HCEC-1CT) were carried out. The results showed a significant concentration dependent reduction of cell membrane fluidity of both PA and OA in the cancer cell line. This effect was not seen in the HCEC-1CT cell line. Overall, there was no significant difference noticeable in the expression of Piezo1 after treatment with PA and OA. However, there was a very significant increase in actin in the cytoskeleton in both cell lines and for both high and low concentrations of PA and OA. For all treatments and both cell lines higher levels of YAP1 were observed in the nucleus than in the cytosol. Significant reduction of YAP1 could be determined for low concentrations of PA in the nucleus in the HCT 116 cell line and a significant increase of YAP1 for higher concentrations of both PA and OA. Low concentration of OA significantly reduced YAP1 in the nucleus of the HCEC-1CT cell line. Interestingly there was a very significant difference in the controls when the two cell lines were compared to each other, both in the expression of YAP1 in the nucleus as well as in the cytosol. To interpret these findings

additional experiments such as shear stress experiments and proteomics are needed to better understand the effects of PA and OA on the intestinal tract with respect to mechanotransduction.

Zusammenfassung

Mechanotransduktion ist die Umwandlung von mechanischen Reizen in biologische Signale. Alle lebenden Organismen werden durch mechanische Kräfte in ihrer Umgebung beeinflusst, die über die sensorischen Systeme zum Überleben beitragen. Ausgehend von der Vorstellung, dass sich unser Körper an die Ernährung und den Lebensstil anpassen kann, haben wir untersucht, ob die Exposition gegenüber Fettsäuren die Physiologie der Darmzellen und insbesondere die Mechanotransduktion beeinflussen kann. Bei der systematischen Analyse des mechanosensorischen Apparats der Zellen postulierten wir eine Beteiligung mehrerer Elemente: Erstens Piezo1-Kanäle, bei denen es sich um „mechano-gated“ große Ca2+-permeable nicht-selektive Kationenkanäle handelt. Jüngste Erkenntnisse deuten darauf hin, dass Piezokanäle bei pathophysiologischen Prozessen wie Darmentzündungen, Krebserkrankungen und kardiovaskulärer Mechanobiologie eine Rolle spielen. Darüber hinaus ist das Yes-assoziierte Protein 1 (YAP1) ein Co-Transkriptionsfaktor in einer Reihe von biochemischen Prozessen, die die Organgröße, Regeneration und Tumorentstehung regulieren. Darüber hinaus stellt YAP1 bei einigen Krebsarten ein starkes Onkogen da, und daher ein potenzielles Ziel bei der Behandlung von Krebs. Sowohl Piezo1 als auch YAP1 sind für ihre Funktion von mechanischen Reizen abhängig. Da Palmitinsäure (PA) und Ölsäure (OA) zu den häufigsten Fettsäuren bei der Nahrungsaufnahme gehören und ebenfalls zu den Lipidbausteinen, von denen bekannt ist, dass sie die mechanischen Eigenschaften der Membran verändern, lautet die Hypothese, ob diese Fettsäuren zu einer Veränderung der Fluidität der Zellmembran, zu einer unterschiedlichen Verteilung der Piezo1-Kanäle, zu einer Veränderung des Zytoskeletts bezüglich Aktin oder zu einer Veränderung der Translokationseffizienz von YAP1 führen könnten. Es wurden Experimente mit einer menschlichen Dickdarmkrebs-Zelllinie (HCT 116) sowie einer menschlichen immortalisierten epithelialen Darm-Zelllinie (HCEC-1CT) durchgeführt. Die Ergebnisse zeigten eine signifikante konzentrationsabhängige Verringerung der Zellmembranfluidität sowohl von PA als auch von OA in der Krebszelllinie. Dieser Effekt wurde bei der HCEC-1CT-Zelllinie nicht beobachtet. Insgesamt war kein signifikanter Unterschied in der Expression von Piezo1 nach der Behandlung mit PA und OA festzustellen. Allerdings war bei beiden Zelllinien und sowohl bei hohen als auch bei niedrigen Konzentrationen von PA und OA ein sehr deutlicher Anstieg von Aktin im Zytoskelett zu beobachten. Bei allen Behandlungen und beiden Zelllinien wurden höhere YAP1-Konzentrationen im Zellkern als im Zytosol beobachtet. Bei der Zelllinie HCT 116 konnte bei niedrigen Konzentrationen von PA eine signifikante Verringerung von YAP1 im Zellkern und

bei höheren Konzentrationen von PA und OA ein signifikanter Anstieg von YAP1 festgestellt werden. Niedrige Konzentrationen von OA reduzierten YAP1 im Zellkern der HCEC-1CT-Zelllinie signifikant. Interessanterweise gab es einen sehr signifikanten Unterschied in den Kontrollen, als die beiden Zelllinien miteinander verglichen wurden, sowohl in der Expression von YAP1 im Zellkern als auch im Zytosol. Um diese Ergebnisse zu interpretieren, sind zusätzliche Experimente wie „Shear-Stress"-Experimente und Proteomik erforderlich, um die Auswirkungen von PA und OA auf den Darmtrakt im Hinblick auf die Mechanotransduktion besser zu verstehen.

Acknowledgements

I would like to thank my supervisor Ass.-Prof. Giorgia Del Favero for her valuable insights and contagious enthusiasm while guiding me throughout the entire Master project. I would like to thank Endre Kiss MSc. Ph.D. for teaching me cell culture and imaging techniques. I am grateful to Maximilian Jobst MSc. for introducing me to Origin Pro – statistics have become a lot more fun. I would like to thank Univ.-Prof. Doris Marko, who kindly provided the cell lines to make the research possible. Last but not least I want to express my deep gratitude to the ones I love - especially Jonathan, Mia, Jordan, Trent, and Mom - for their support on this journey.

Abbreviations

ADP: adenosine diphosphate

ATP: adenosine triphosphate

benzene sulfonate

CER: cerulenin

CVD: cardiovascular disease

DEG/ENaC/ASIC:

DMSO: dimethyl sulfoxide

EC: enterochromaffin

ECM: extracellular matrix

FAK: focal adhesion kinase

FASN: fatty acid synthase

GPCRs: G-protein coupled receptors

h: hours

HCEC-1CT: Immortalized human colonic epithelial cells

HCT 116: human colon carcinoma cells

IBS: irritable bowel syndrome

LATS 1/2: large tumour suppressor

LCI: live cell imaging solution

min: minutes

MST 1/2: STE20-like kinase

OA: oleic acid

PA: palmitic acid

PDA: pyrene-dodecanoic acid

ROI: region of interest

T2D: type 2 diabetes

TEAD:

TMC/TMHS/TMIE:

WST-1: tetrazolium salt

YAP: Yes-associated protein

Contents

List of Figures

1.**Introduction**

All living organisms are affected by mechanical forces in their environment, which ultimately contribute to survival through the sense of touch, proprioception, hearing, balance, and pain [1]. Beyond the functions in the sensory systems, mechanical forces are involved in numerous physiological functions such as vascular tone, flow sensing in the kidneys or secretion in the intestine [2]. The conversion of mechanical stimuli into biological signals is known as mechanotransduction [3]. Mechanotransduction relies on a complex sensory apparatus and the discovery of mechanosensitive ion channels and transcription factors led to the understanding that mechanotransduction plays an important role for optimal functioning of biochemical pathways, that when perturbed, pathophysiological conditions can arise [4, 5]. In the intestine the epithelium is constantly exposed to external forces such as the stretch and compression stemming from peristaltic movements and furthermore withstands shear stress caused by the flow of luminal contents [6]. The intestinal epithelium is the fastest self-healing tissue in adult mammals, as it only takes 3 – 5 days from the stem cell niche to extrusion [7]. It consists of a monolayer of cells that creates a lining on the inner surface of the gut. The intestinal epithelium acts as the first physical barrier against the environment and simultaneously absorbs water, nutrients, and ions. Invaginations referred to as crypts and protrusions called villi originate through folding of the monolayer [6]. Stem cells reside at the bottom of the former, where they encounter biochemical signals to maintain their self-renewal [8]. Through the invaginations they are largely protected by potentially harmful luminal content. On the other hand, villi have a large surface area to optimize absorption and are perpetually exposed to luminal constituents. Through signalling molecules stem cells continuously divide, leave the stem cell niche, and thereafter move to the crypt neck [9]. Here the cells proliferate even faster as transit amplifying cells. These in turn either differentiate into secretory (enteroendocrine cell, tuft cells, goblet cells) or absorptive (enterocytes) cells, in a span of approximately two days. The differentiated cells mature during migration toward the tip of the villus, where they are then extruded and die [7]. Besides the aforementioned external mechanical stimuli such as stretch, compression, and shear stress to which the epithelium is exposed, mechanical tasks must be performed by the intestinal epithelium itself to maintain homeostasis. These include preservation of barrier integrity, cell proliferation and extrusion, upkeep of tissue folding, transformation by crypt fission and fusion, migration between tissue compartments and partitioning of cell types [6].

1.2 The Cell Membrane and Cytoskeleton

Fatty acids are the lipids' building blocks and are an integral part of the cell membrane. As interface with the extracellular environment the structure and composition of the cell membrane contribute to the optimal functioning of signalling induced by mechanotransduction through fluidity or rigidity caused by the membranes' components [10, 11]. The "force-from-lipids" principle establishes that the mechanical properties of the membrane ultimately control the conformational rearrangements underlying mechanosensitive ion channel gating allowing the cell to convert mechanical stimuli into electrical and biochemical signals [12]. Another current model for mechanoelectrical transduction is the "force from filament" principle, in which channels or the plasma membrane, are directly connected to cytoplasmatic as well as extracellular matrix (ECM) tethers and bring about conformational changes and channel gating [12, 13]. This demonstrates that the cytoskeleton plays a crucial role in mechanotransduction.

1.3 Mechanosensitive Piezo1 and YAP1

There has been discussion as to what properties an ion channel must exhibit to qualify as a transducer of mechanical force. It has been suggested that the candidate gene of an ion channel must be expressed in a mechanosensitive cell. Should the gene be deleted, it would lead to the loss of mechanosensitivity of the cell, but not affect the development of the cell. The candidate gene should also code for the pore-forming sub-unit. This could be validated through structural analysis or by engineering point mutations which lead to changes in ion selectivity and conductance [2]. This holds true for Piezo1 and Piezo2 which both have proven to be mechanosensitive Ca^{2+}-permeable non-selective cation channels [14] involved in numerous processes in the intestinal tract [15]. Recently yes-associated protein (YAP), and transcriptional coactivator with PDZ-binding motif (TAZ), was shown to exhibit mechanotransductional properties [16]. Studies have demonstrated that YAP/TAZ are controlled by numerous factors such as endoplasmic reticulum (ER) stress, cell density, hypoxia, growth factors, osmotic stress, cell adhesion, energy stress, mechanical force, Wnt and a considerable number of G-protein-coupled receptor (GPCR) ligands. Furthermore, it is palpable that YAP/TAZ are highly susceptible to environmental conditions i.e., nutrition/metabolites [17]. Although most research on YAP/TAZ has focused on the area of differentiation and cell growth, the knowledge in the field of YAP/TAZ in metabolism regulation in growth and tissue homeostasis is advancing

swiftly. Here the effects of palmitic acid and oleic acid on the mechanosensory apparatus will be assessed *in vitro* using intestinal cell lines.

1.4 Aim of this Thesis

Since fatty acids are the lipids building blocks and are known to alter the mechanical properties of the membrane, the central aim of this thesis is whether dietary lipids can affect mechanotransduction. This could be obtained, firstly by the modification of cell membrane fluidity, secondly either and/or through a variation of the distribution of the Piezo ion channels and thirdly through a variation of the translocation efficiency of mechano-sensitive transcription factor YAP1. To follow these demands, two intestinal cell lines are chosen. One being a tumorigenic cell line (HCT 116) and one being an immortalized epithelial cell line (HCEC-1CT). Through the incorporation of both palmitic acid and oleic acid into the cell membrane and the application of cerulenin, the effects of all three compounds on membrane fluidity, expression of the Piezo1 ion channel, actin in the cytoskeleton and the translocation of YAP1 will be assessed.

2 Theoretical Background

2.1 Mechanotransduction

Living organisms respond to their environment down to the cellular level. Cells are constantly subjected to chemical or physical stimuli which have an effect on the organism through various biochemical pathways [18]. Mechanical forces are perpetually exerted on the epithelial cells of the vascular system through the cardiac pump which circulates a large volume of blood throughout the body causing a cycle of stretching and relaxing of force variations on the cells [5]. Similarly, in the process of breathing, continuously varying levels of mechanical forces are applied to the epithelial cells which line the lung [19]. In the intestinal tract peristalsis is involved in the uptake, and transport of food from the mouth to the excretion of waste through the rectum. Here too mechanical forces are applied throughout the intestinal tract through the undulating movement of the muscles and the passage of chyme [6, 15]. Furthermore, the role of mechanical force is of great importance in embryonic development in regard to organogenesis, displaying the significance of the cell and it's interaction with the microenvironment – neighbouring cells and the extracellular matrix - through mechanotransduction [20]. Early twentieth century D'Arby Thompson's pioneering work "On Growth and Form" led to the emerging field of the intersection between morphogenesis and the physical sciences as well as mathematics [21]. Since then, research has shown that mechanotransduction is involved in numerous processes such as proliferation, cell differentiation, motility, and protein synthesis [22]. The absence of or deficiency of mechanical cues can lead to pathophysiological changes which can cause dysfunction and disease [5]. Understanding cell migration, ion channel activation via shear stress and the discovery of the integrin proteins in the 1980s as well as the emergence of new techniques such as live cell imaging and the development of assays has advanced research in the field of mechanotransduction [2, 23, 24]. There are different types of force that can be applied to cells in assays to better understand the process of mechanotransduction. These are among others shear stress, stretch, suction stretch, mechanical indentation, and osmotic change-induced swelling [2]. One type of mechanosensor that has been identified over the last two decades are mechanosensitive ion channels consisting of several gene families which include DEG/ENaC/ASIC Ion Channels, Transient Receptor Ion Channels, TMC/TMHS/TMIE: Transduction Channel in hair cells, Mechanosensitive Potassium Channels and Piezo Ion

Channels [2]. Other candidate mechanosensors which play an important role are cell-cell adhesion complexes [25], the glycocalyx [3], focal adhesion sites and their corresponding proteins [26], and the cell membrane [10].

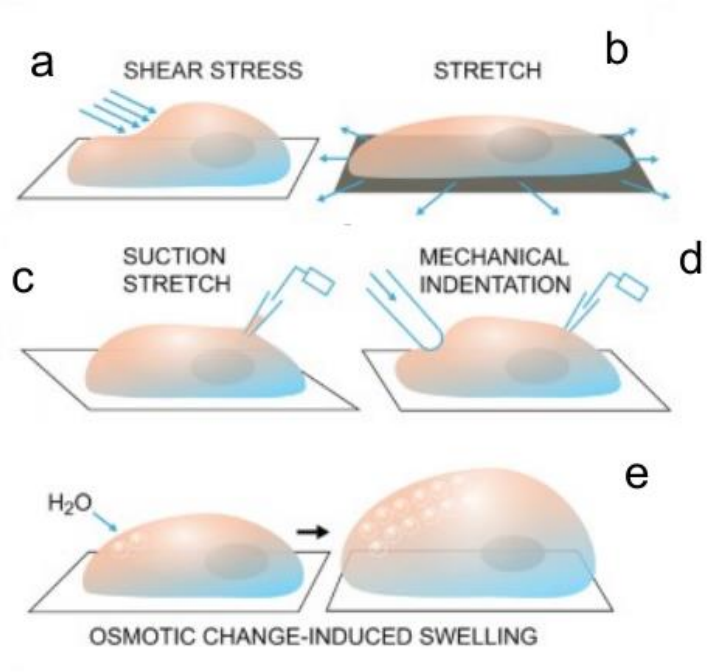

Figure 1: A selection of types of force that can be applied to cells.

a: shear stress; b: stretch; c: suction stretch; d: mechanical indentation; e: osmotic change-induced swelling. Taken and adapted from Ranade et al. 2015.

2.2 Cell Membrane

The cell membrane consists of a fragile two-ply sheet of lipid molecules approximately 5 nm thick which acts as a protective sheath which ensures that cells can survive and grow. The lipid-bilayer is mainly composed of amphipathic molecules, with phosphatidylcholine being the most prevalent [27]. Although the membrane acts as a permeability barrier to most water-soluble materials, highly selective channels and transporters permit the import and export of substances such as nutrients, metabolites, and ions through the membrane [28]. Regular packing of the hydrocarbon tails results in closeness between the molecules which leads to an increase in viscosity as seen in saturated fatty acids. Unsaturated fatty acids have kinks in their tails due to the double bonds and cannot be packed as closely resulting in a more fluid membrane [29]. Cholesterol which comprises for about 20 % of the total lipid weight in membranes also has a modulating effect, mostly leading to an increase in stiffness and a decrease of permeability [30].

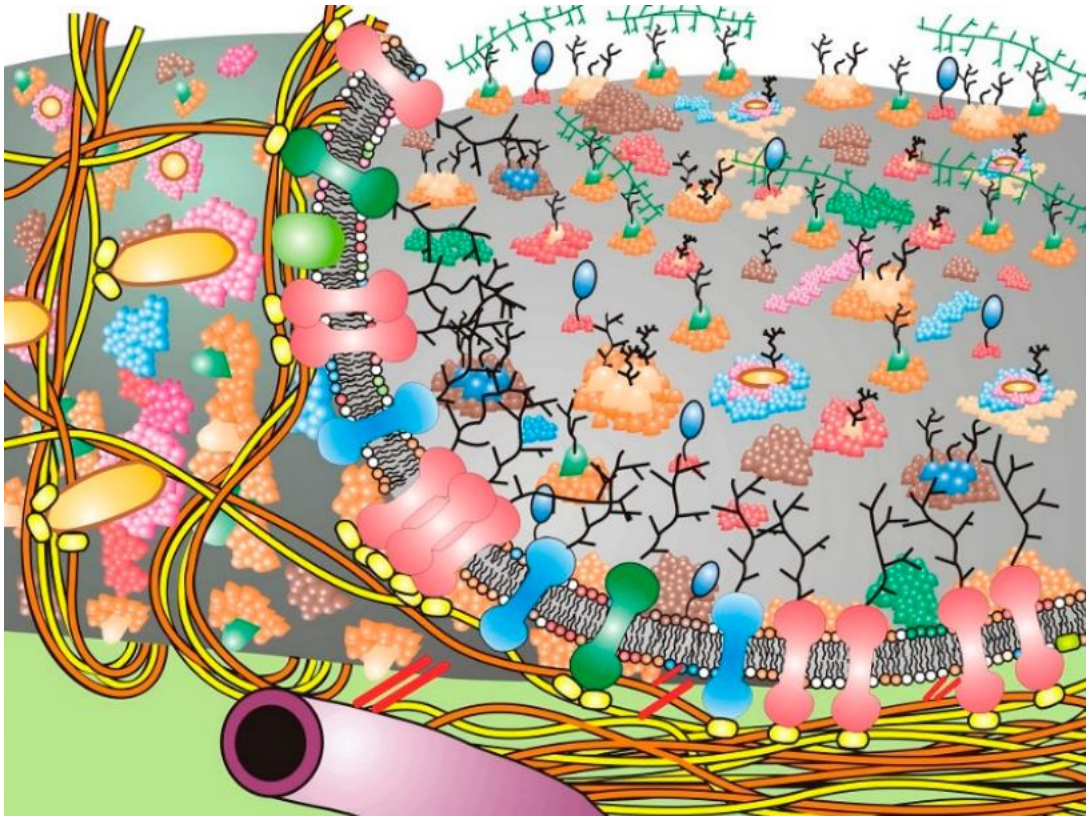

Figure 2: The structure of the cell membrane.

Taken from Nicolson, G. L et al., 2021. This figure represents an updated version of the Singer-Nicolson Fluid-Mosaic Membrane model to depict the complexity of the cell membrane structure. Molecules and other structures are not shown proportionately

The cell membrane is not a rigid structure but can be regarded as a flexible two-dimensional fluid, originally based upon the Singer-Nicolson Fluid-Mosaic Membrane model of the cell membrane as proposed in 1972 [27], however continued research has shown that this original scheme does not reflect the heterogeneous complexity now applicable to the cell membrane. Among numerous advancements to the model are the discovery of transbilayer lipid motions, the fact that membranes are curved and the lateral heterogeneity of membranes. So, under conditions which entail spatial and temporal limitations, membrane lipids may be subjected to "flip-flop" or fast transbilayer motion. Also, domains or heterogeneous patches comprise areas of approximately 0,1 – 1,0 µM, which are enriched with certain proteins and lipids contributing not only to characteristic structural but also functional properties [31]. Furthermore, membrane curvature is not a fixed parameter, but can dynamically be modulated by protein binding and protein insertion as well as changes in lipid composition. Of great importance to membrane curvature is the geometry of the lipids, including the concepts of lipid packing – as mentioned before, monolayer intrinsic curvature and membrane intrinsic curvature. If a membrane was only comprised by laminar lipids, it would function as an insulator but would not be able to

support life [31]. Having non-laminar lipid structures present in the membrane makes it possible to respond to stimuli, because the membrane is able to be disrupted through electrical and chemical gradients or through the insertion of proteins [31, 32]. Mechanical properties of the cell membrane allow for cell growth and division by adding membrane with no loss of continuity and self-healing properties ensure immediate closing of the cell membrane if damaged [31]. The cell membrane has an important role in that it serves as an anchor for macromolecules on both the extracellular as well as on the cytosolic side [31]. Furthermore, functional proteins distributed throughout the membrane give the membrane it's individual characteristics and are classified as peripheral, integral [27, 33] or membrane associated proteins. These often function as sensors or receptors to appropriately respond to the environment.

2.3 Piezo Ion Channels

Mammalian Piezo1 and Piezo2 have recently been discovered with each forming large Ca^{2+}-permeable non-selective cation channels. These ion channels have abilities to sense and respond to mechanical forces such as membrane stretch [14], hence the name "Piezo" is derived from the Greek word *piezein*, meaning to "press". Both Piezo1 and Piezo2 are involved in physiological processes that are essential to life. In the mouse Piezo1 plays a role in the development of the lymphatic as well as the vascular system [34, 35]. Piezo2 plays an important role in mechanotransduction and is found in the sensory neurons of Merkel cells and the dorsal root ganglia [34]. Piezo2 is also present in the enterochromaffin cells (EC) of the intestinal tract [36]. Genetic ablation of either Piezo1 or Piezo2 leads to embryonic or early post-natal lethality in mice [34]. In humans a suppression of Piezo2 is associated with a loss of normal touch sensation and proprioception [37]. The vast array of physiological functions that Piezo channels contribute towards in living organisms have yet to be fully understood. Recent findings suggest that Piezo channels play a role in pathophysiological processes including migraine headaches [38], gut inflammation [39], cancers [4], cardiovascular mechanobiology [35] and gastric cancer[40]. Piezo2 has been suggested as a candidate biomarker for irritable bowel syndrome (IBS) and gut inflammation [39, 41].

To determine the structure of a Piezo channel cryo-electron microscopy (cryo-EM) was used. It was found that Mouse Piezo1 has a trimeric three-bladed, propeller-like shaped structure [42].

It forms a pore-forming ion channel which is directly gated by membrane stretch. This central pore-forming module consists of an inner helix (IH), an intracellular C-terminal domain (CTD) an outer helix (OH) and a C-terminal extracellular domain (CED). The peripheral regions are composed of "blade", "beam" and "anchor" domains. The "blade" domains are extracellular and have 36 peripheral helices (PHs) in each sub-unit. The "beam" and "anchor" domains are intracellular (figure 3a). It has been suggested that the N-terminal non-pore containing region transmits mechanosensitivity on the channel [34],[43]. Piezo2 channels are large membrane proteins comprised of over 2,800 residues, but share only about 42% sequence homology with Piezo1, although the overall structure is very similar [44]. Through single channel recordings, it was discovered, that an intrinsically disordered domain next to the beam acts as a cytostolic plug. This plug limits ion permeation probably by clogging the inner vestibule not only in Piezo2 but also in Piezo1 [45]. Through structural comparison between Piezo1 and Piezo2, Wang *et al*. discovered that the transmembrane constriction site is controlled by the cap domain and might act as a transmembrane gate [46].

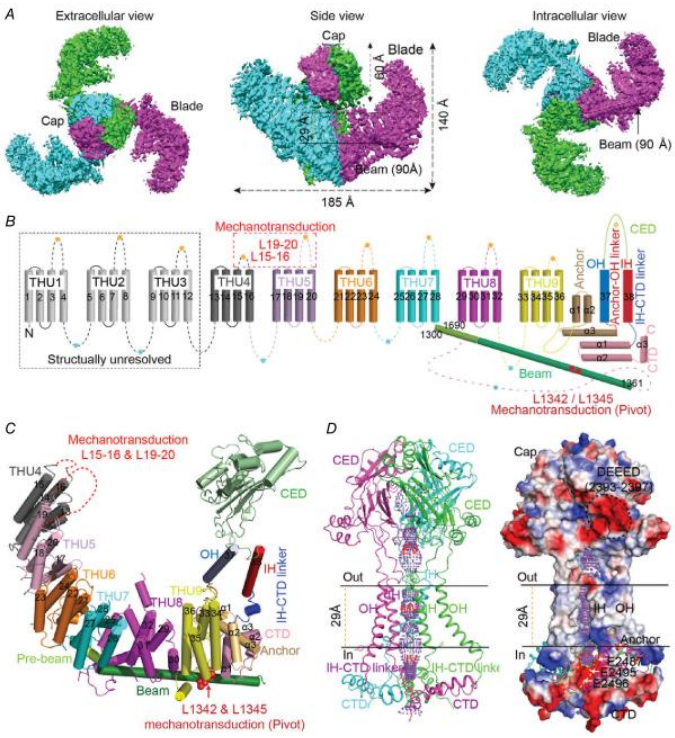

Figure 3: Structure of mouse Piezo1

A: *depicts the trimeric three-bladed, propeller-like shaped structure made up of cap and blades.* ***B:*** *represents a 38 transmembrane topology model: individual THUs (transmembrane helical units) as well as major structural domains are labelled; Areas functionally important for mechanotransduction are labelled in red.* ***C:*** *a cartoon model showing one sub-unit with structural domains labelled.* ***D:*** *a ribbon*

diagramme of the the ion-conducting pore unit (left). Surface electrostatic potential is shown on the right. Taken from Zhao et al., 2018 and Beech et al., 2018.

2.4 Actin and the Cytoskeleton

The cytoskeleton of the eucaryote cell spans the cytoplasm and connects the nucleus with the plasma membrane. The cytoskeleton is dynamic and provides the cell with remodelling capabilities through molecular motors acting on it and also allows for active transport within the cell [47]. Further dynamic properties of the cytoskeleton are aiding during cell division, assisting the cell respond to its environment and being responsible for movement of the cell. This includes processes such as engulfing particles through phagocytosis, wound healing, and muscular movement [48]. Additionally, the cytoskeleton controls the location of organelles in the cell [49]. The protein filaments can be divided into intermediate filaments, microtubules, and actin filaments. Intermediate filaments mostly provide structural support, whereas microtubules and actin facilitate faster cell responses [47]. Approximately 5 % of total protein in the cell is actin of which half are globular and half assembled into filaments. These filaments (F-actin) are helical polymers assembled spontaneously from globular actin (G-actin) monomers which have a flexible structure with a diameter of 7 nm and a few microns in length. Most filaments are capped before reaching a length of 0,5 µm [49]. Individual micro-filaments are not only flexible but also highly dynamic and can form stress fibers or more mechanically stable bundles [50]. Actin has the ability to bind and hydrolyse ATP. The dynamic turnover of actin filaments is due to the conformational change through the transition from ATP-actin to ADP-bound actin [51]. A dynamically regulated actomyosin network can be achieved through the cross-linking of myosin molecular motors and actin filaments. This enables cell motility and application of force through localized contractions of the network, but also facilitates local transport along filaments. Focal adhesions are stable cell-matrix connections of clustered trans-membranal integrins, which connect to the actin-network and are responsible for transmitting localized forces extracellularly [47].

If forces and deformations are applied to the cell it is the cytoskeleton that is important for maintaining the cell's stiffness and morphology as well as ensuring plasma membrane integrity and stability. Actin typically localizes to the submembranal region or cortical region and so supports the plasma membrane against deformations, but also facilitates formation of

lamellipodia or filopodia [52]. Changes in the cytoskeleton which lead to reduced internal and external stiffness can be seen in cancer cells [53]. Here a reduction in cortical actin as well as stress fibers and F-actin filaments can be observed, resulting in a weaker cytoskeletal structure [54].

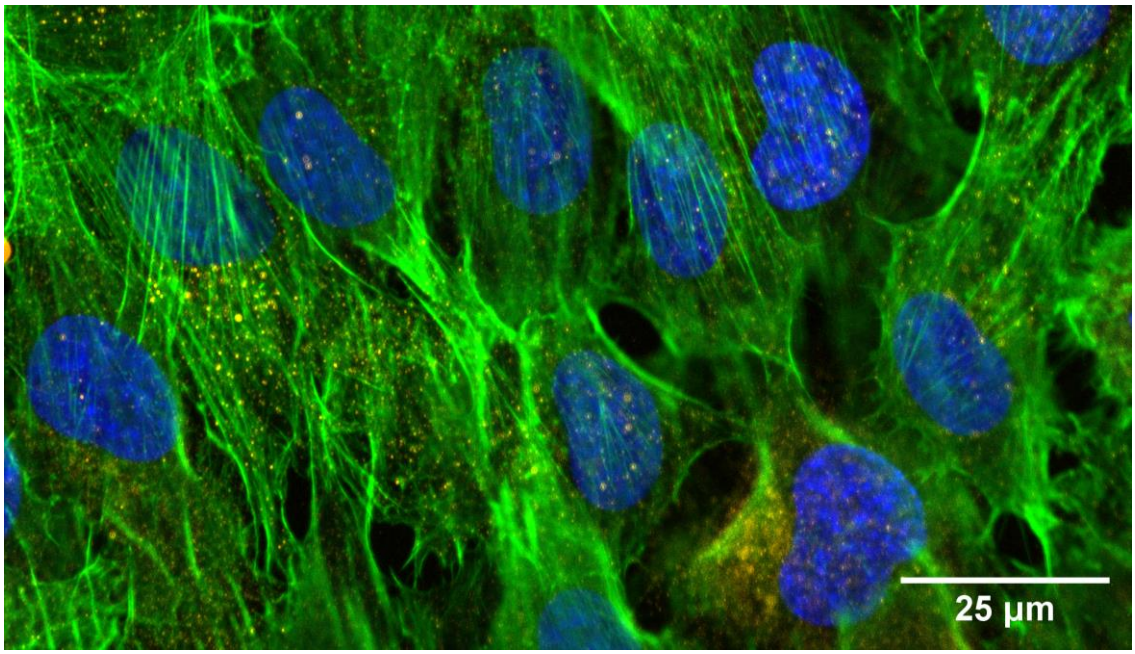

Figure 4: Actin filaments in HCEC-1CT cells

Actin filaments are stained by phalloidin and depicted in green, nuclei in blue. Image was taken with LSM Zeiss 710 equipped with ELYRA PS.1 system with a Plan Apochromat 63X/1.4 oil objective.

2.5 YAP1 Transcription Factor

Yes-associated protein 1 (YAP1) is a transcription coregulator and component of the hippo signalling pathway which regulates organ size through cell proliferation and apoptosis [55]. Recently YAP/TAZ have been identified as mechanotransducers, relaying mechanical stimuli from the nucleus [16]. YAP and TAZ are largely equivalent proteins based on their genetic redundancy and structural similarities, however they do display different phenotypes and investigating these differences are an ongoing process, but they have previously often been merged as YAP/TAZ [56]. YAP can be regulated both biochemically and mechanically. Biochemically YAP is regulated by the hippo signalling pathway and mechanically by cues such as strain, shear stress, ECM rigidity or adhesive area [57]. The hippo pathway consists of a cascade of interacting kinases mammalian STE20-like kinase (MST 1/2) and large tumour

suppressor (LATS 1/2), which eventually lead to the phosphorylation of YAP/TAZ at the serine-127 residue [58]. This leads to YAP/TAZ remaining in the cytoplasm, whereas if the hippo signalling pathway is switched off due to the loss of polarity, YAP/TAZ is not phosphorylated at ser-127 and can pass into the nucleus where it promotes numerous transcriptional programmes involved in cellular proliferation, invasion and suppression or expression of apoptotic genes [56]. Though as a transcriptional co-activator not binding directly to the DNA, YAP modulates gene expression depending on its binding partner. Therefore, YAP can either act as a tumour suppressor by binding to for example p73 in the nucleus and expressing apoptotic genes [59] or as an oncogene through its interactions with TEA domain (TEAD) transcription factors [60].

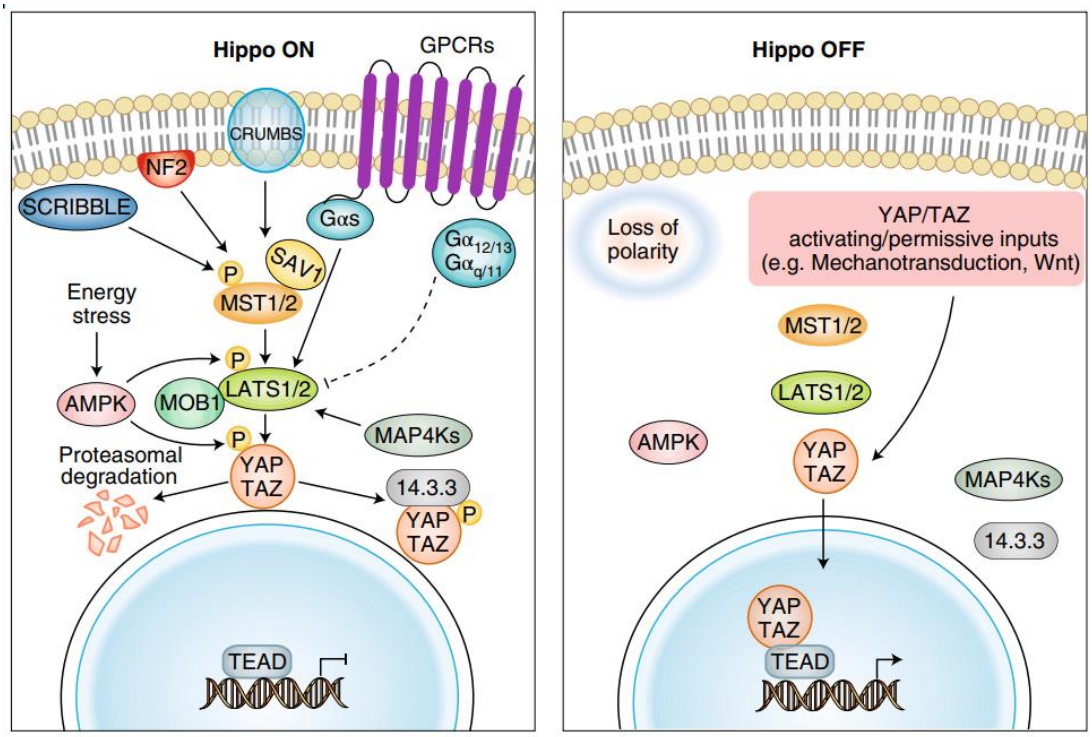

Figure 5: The Hippo pathway

The Hippo pathway in ON state (left): YAP/TAZ is phosphorylated by LATS 1/2 and cannot enter the nucleus. The Hippo pathway in OFF state (right): YAP/TAZ is not phosphorylated and can enter the nucleus to function as a transcription factor. Taken from Totaro et al., 2018

The process of YAP nuclear translocation can additionally be achieved independently of the hippo signalling pathway. It has been proposed, that through linker of the nucleoskeleton and cytoskeleton (LINC)-related nuclear stretching, resulting in the increased permeability of the nuclear pores, leads to entry of YAP/TAZ into the nucleus. In other words, mechanical coupling between the nucleus and cytoskeleton is necessary for YAP nuclear translocation. This is

accomplished through exposure to a stiff environment in which cells build a mechanical network between the cytoskeleton and the nucleus, which allows for forces exerted through focal adhesions to extend to the nucleus. This leads to nuclear flattening, which in turn stretches the nuclear pores and increases YAP nuclear import through the pores' reduction of resistance to molecular transport [57]. These are only two of many emerging signal routes through which YAP/TAZ can be activated or deactivated. Moreover, the Wnt-pathway coordinates both ß-catenin and YAP/TAZ activity [56]; different classes of G-protein coupled receptors (GPCRs) function as repressors or inducers of YAP/TAZ [61]. Furthermore, the regulation of YAP/TAZ is linked to metabolic factors such as the metabolism of lipids through the mevalonate/cholesterol pathway leading to the promotion of proliferation [62] or through the presence of the enzyme of the rate limiting step of the glycolytic cascade – phosphofructokinase 1 – which stabilizes the interaction between YAP/TAZ and TEAD and therefore promotes the transcriptional programme [63]. Beyond these there are many more pathways that interact or are affected by YAP/TAZ and research in this field is continuously growing with promising applications in cancer through bioengineering [20].

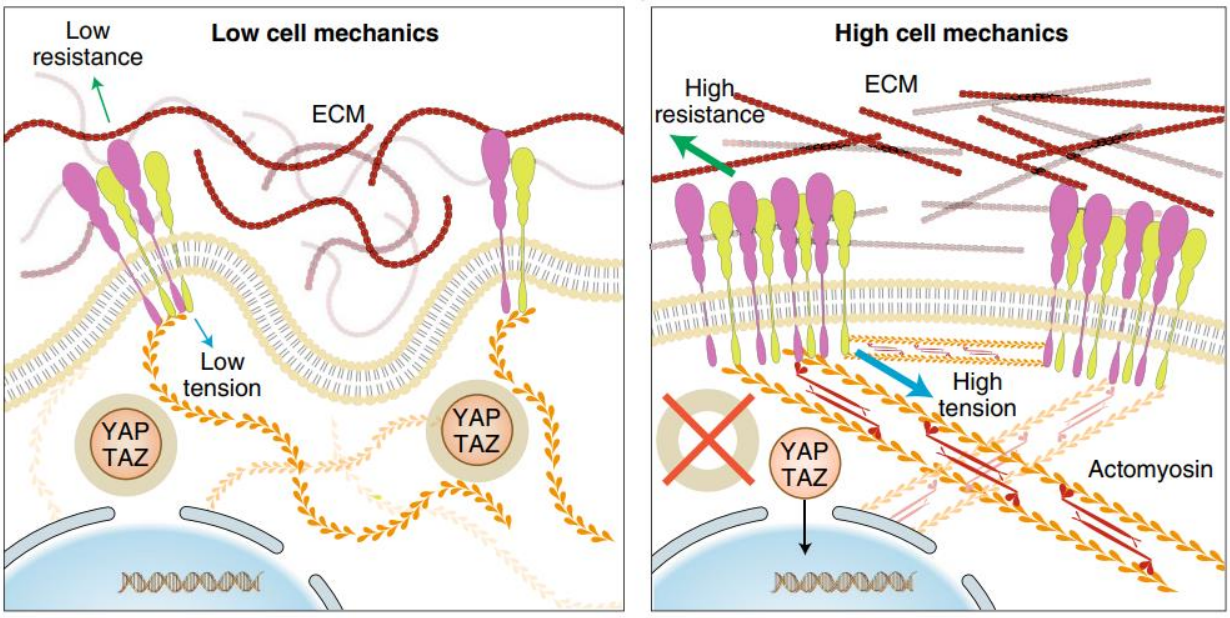

Figure 6: Low and high cell mechanics

By adjusting their tensional states through integrin-mediated cell-ECM adhesions, cells respond to ECM rigidity. Low ECM resistance (left) leads to reduced adhesion, low actomyosin contractility and YAP/TAZ inactivation. High ECM resistance (right) leads to integrin clustering and intracellular tension incapacitating YAP/TAZ mechanically regulated inhibitory mechanisms, permitting YAP/TAZ function. Taken from Totaro et al., 2018

2.6 Dietary Constituents and Modulation of Mechanotransduction

Fatty acids are the lipids building blocks and play an important role the structure of membranes [27]. Fatty acids are also a source of energy which the organism can access through the production of acetyl-CoA by means of ß-oxidation in the matrix of mitochondria and peroxisomes [64]. Fatty acids exhibit different properties depending on their chain length and the degree of saturation [65].

Palmitic acid is a fatty acid which is saturated and 16 carbon atoms in length. It belongs to one of the most prevalent fatty acids in the human diet and can be found in products such as palm oil (44% of fats), butter, milk, cheese, and meats such as beef [66]. PA can be derived from dietary sources but can also be endogenously produced from other fatty acids, amino acids, or carbohydrates. PA constitutes for 20 - 30 % of total fatty acids in adipose triacylglycerols (TAG), and membrane phospholipids (PL) [67]. The tissue concentration of PA does not significantly change [68] due to higher intake of PA, due to the fact, that intake is abrogated by PA endogenous synthesis via *de novo synthesis* (DNL). However, if DNL is strongly induced through factors such as nutritional constituents and certain physiopathological conditions, an increase in tissue content of PA and disruption of homeostatic control of its tissue concentration is observed [69]. Research has shown that PA not only contributes as a source of energy but also functions as an intracellular signalling molecule which plays a role in the development of cancers and furthermore advances the metastatic potential of breast cancer and melanoma in a CD-36 (fatty acid receptor) dependant manner [70] and promotes the growth of prostate cancer [71]. Furthermore, a high fat diet, which coincides with a high uptake of saturated fatty acids is associated with numerous diseases such as cardiovascular disease (CVD), type 2 diabetes (T2D), metabolic syndrome and contributes to an increase in morbidity and total mortality [65].

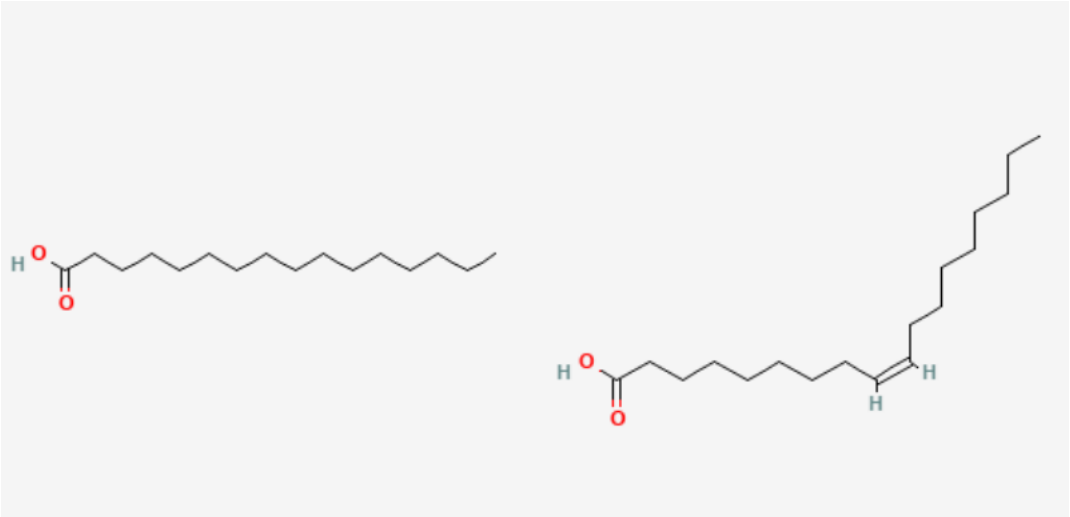

Figure 7: Palmitic acid and oleic acid

Chemical structures of palmitic acid (left) and oleic acid (right). Source: Pubchem (https://pubchem.ncbi.nlm.nih.gov/compound)

Oleic acid is a monounsaturated fatty acid (MUFA), with one double-bond in position 9 (ω-9 FA) and is 18 carbon atoms in length. OA has been associated with positive health effects such as lowering blood pressure and blood glucose, antioxidant and anti-inflammatory effects, improving lipoproteins, promoting wound healing and inhibiting cell proliferation in cancer [72]. Furthermore, in HT29 cells it was shown that olive oil as well as oleic acid can significantly induce apoptosis in the colorectal cancer cell line [73]. As PA, so OA belongs to the most prevalent of fatty acids in the human diet. Olive oil is an excellent source of OA constituting about 75 % of total fatty acids and an important ingredient of the traditional Mediterranean diet which has various health benefits [74]. Two cohort studies - the Nurses' Health Study investigating 83 349 women (1980 – 2012) and the Health Professionals Follow-up Study investigating 42 884 men (1986 – 2012) – taking diverse lifestyle factors into consideration, assessed among others the influence of the intake of dietary fat (assessed at baseline and updated every 2 – 4 years) on total mortality. All individuals were free of, cancer, types 1 and 2 diabetes and cardiovascular disease at baseline. It was shown that higher intakes of polyunsaturated fatty acids (PUFA) and MUFAs were associated with lower mortality, whereas saturated fatty acids and *trans*-fat had the opposite effect (figure 8). It was concluded that replacing 5 % of energy from MUFA and PUFA was associated with a decrease in total mortality by 13 % and 27 % respectively [65].

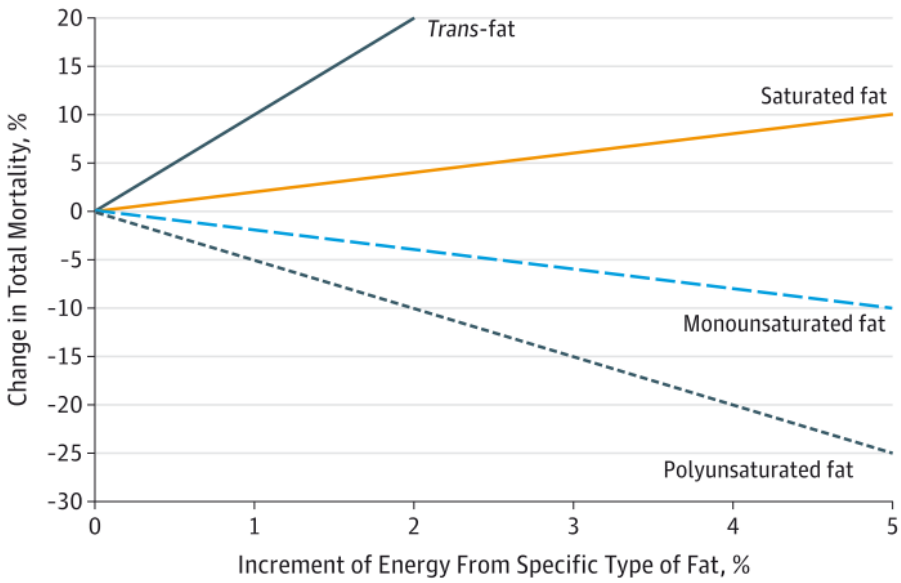

Figure 8: Percentage of Energy from specific types of fat and the change in total mortality

Percentage of Energy from specific types of fat and the change in total mortality. These data are based on the Nurses' Health Study and the Health Professionals Follow-up Study Taken from Wang et al., 2016

3 Materials and Methods

3.1 Materials

The complete list of chemicals, consumables, software, and devices utilized for this work is shown in tables 3 - 6 in the appendix. Here the compounds and the two cell lines used for the experiments will be presented.

3.1.1 Fatty Acids and FASN Inhibitor

Cerulenin: Beside PA and OA (previously discussed) another compound in use is cerulenin ((2R, 3S)-2,3-epoxy-4-oxo-7,10-trans,trans-dodecadienamide) [75]. This is an antibiotic and antifungal agent originally isolated from *Cephalosporium caerulens*. This product is synthetically derived [76]. The compound acts as a potent and specific Fatty Acid Synthase (FASN) inhibitor and has been shown to block the synthesis of stearoyl-CoA and eicosanoyl-CoA fatty acids in microsomes. Cerulenin binds covalently to the active centre cysteine of the condensing enzyme domain and inhibits FASN [77].

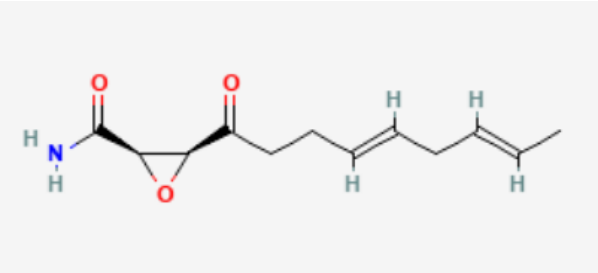

Figure 9: Cerulenin

Chemical structure of cerulenin. Source: Pubchem (https://pubchem.ncbi.nlm.nih.gov/compound)

3.1.2 HCT 116

This cell line was acquired from ATCC and will serve as an in *vitro* model for cancerous intestinal cells. There is a mutation on the codon 13 of the ras protooncogene and the cells can be used experimentally among others in toxicology and cancer research. This cell line was

originally isolated from an adult male with colon cancer (www.atcc.org/products/ccl-247). Colorectal cancer is (CRC) one of the most prevalent cancers worldwide, with high rates of morbidity and mortality [78]. The HCT 116 cells are small and rather round in their morphology as can be seen in figure 10.

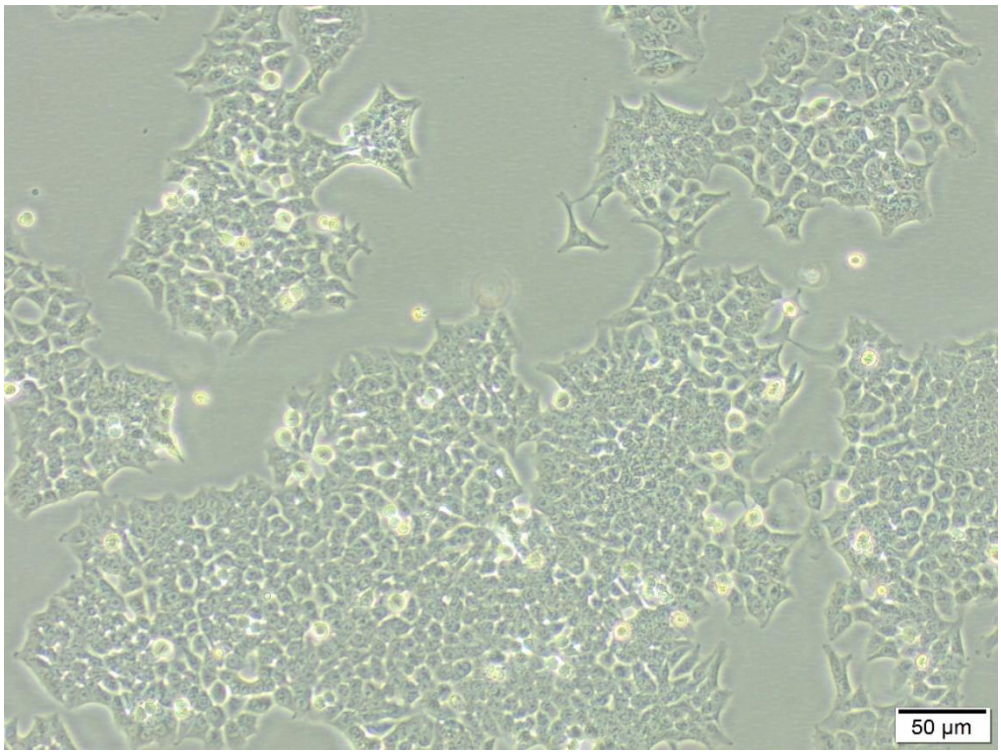

Figure 10: HCT 116 cells

(Image taken with Olympus SC50, 10x magnification).

3.1.3 HCEC-1CT

The HCEC-1CT cell line will serve as an in *vitro* model for normally functioning intestinal epithelial cells. The human colonic epithelial cell (HCEC) cell line was initially derived from biopsies stemming from two different patients ("1" and "2") in 2010. These were immortalized by expression of cyclindependant kinase 4 and the catalytic constituent of human telomerase, allotting the numbers "1" and "2" and the letters "C" and "T" and to complete the abbreviation [79]. In 2D culture the morphology of the HCEC-1CT cells is cuboidal to spindle shaped (figure 11) [79]. These cells were kindly provided by Prof. Jerry W. Shay (UT Southwestern Medical Center, Dallas, TX, USA) [80] and the use kindly allowed by Univ.-Prof. Doris Marko as intramural collaboration.

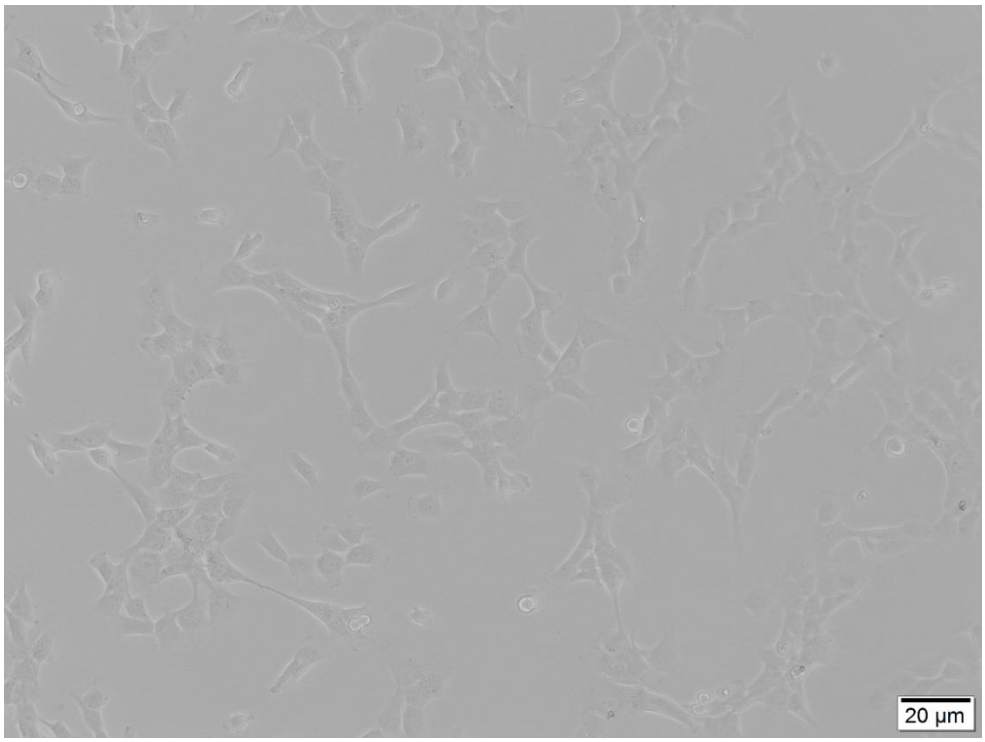

Figure 11: HCEC-1CT cells

(Image taken with Olympus SC50, 20x magnification).

3.2 Methods

The methods implemented in this work will be presented in the following and include cell cultivation and experiments carried out for this thesis.

3.2.1 Cell Cultivation

Cell maintaining: HCT 116 and HCEC-1CT cells are cultivated in flasks in an incubator at 37°C with 5% CO_2. The cells are passaged two to three times per week after reaching a cell confluency of approximately 80 %.

Media composition: The ingredients for the cell culture media for both cell lines can be seen in table 1 and table 2.

Table 1: Composition of the cell culturing medium for HCEC-1CT cells

Agent	Quantity
Dulbecco's Modified Eagle Medium	92,8%
Medium 199 (10x)	2%
Cosmic Calf Serum	2%
1M HEPES buffer solution	2%
Insulin-Transferrin-Selenium [100 µg/ml]	1.04%
Gentamicin Solution	0,12%
Epidermal Growth Factor [100µ/ml] 0.02%	0,02%
Hydrocortison [5 mg/ml]	0,02%

Table 2: Composition of the cell culturing medium for HCT 116 cells

Agent	Quantity
McCoy's 5a medium	89%
Fetal Calf Serum	10%
Penicillin/ Streptomycin Solution	1%

Determination of cell concentration: To determine the number of cells per millilitre Trypan blue exclusion is used. Here the cell membrane permeability increases after cell death and allows inclusion of the dye. Living cells with intact membranes do not incorporate the dye and therefore remain transparent. A 1:2 or 1:5 dilution of cell suspension with trypan blue is prepared and 10 µL are added to a Neubauer cell counting chamber. Living cells are counted under the use of a microscope with 5x magnification in all four squares of the counting chamber. To calculate the concentration of living cells per millilitre, equation (1) is utilized.

$$\frac{cells}{mL} = \frac{mean\ living\ cells * \ dilution\ factor}{chamber\ depth * counted\ area} \qquad (1)$$

3.2.2 Experiments

Preparation of stock solutions and concentrations of compounds: For the application of palmitic acid (Sigma; Lot# SLCH6263) , oleic acid (Sigma-Aldrich; Lot# SLCJ8227) and cerulenin (EMD Millipore Corp, USA; Lot# 3762630) to the cell lines a modified medium was used. Though the recipe is similar to tables 1 & 2, both media do not contain serum and 1mg FA free BSA/mL medium is added to encourage the uptake of the fatty acids which act as hydrophobic small molecule ligands to albumin as a transporter [81]. All three compounds are dissolved in DMSO. To ensure complete solubilization, sonification is used for approximately 30 s. When preparing the stock solutions (500 µM for PA and OA; 100 µM for CER) the DMSO residue is 0,64 % for PA, 0,14 % for OA, and 0,22 % for CER. To ensure equal amounts of DMSO for each concentration, DMSO is added accordingly. Likewise, 0,64 % DMSO is added to serum controls (containing cell culturing medium) and no-serum controls (medium without serum). The concentrations chosen for PA and OA range from 0 µM to 500 µM. This concentration range was chosen on the basis of models previously published [73, 82].

WST-1 Assay

To determine the cytotoxic effect of PA, OA, and CER at different concentrations on the two cell lines, a WST-1 assay was carried out [83-85]. The viable cells are determined by the cleavage of the tetrazolium salt WST-1 (4-[3-(4-Iodophenyl)-2-(4-nitro-phenyl)-2H-5-tetrazolio]-1,3-benzene sulfonate) to formazan through cellular enzymes. The overall activity of mitochondrial dehydrogenases in viable cells increase the amount of formazan dye produced and can then be quantified through spectrophotometric methods [83]. The cells are seeded into a 96-well plate (Sarstedt) and after reaching a confluency of approximately 80 %, the treatment is added and incubated for 24h. The medium is removed, and the cells are washed with phenol red free DMEM and again aspirated. 100µL of WST-1 solution (WST-1:phenol red free DMEM, 1:20) is added to each well and incubated for 30mins at 37°C, 5 % CO_2. Thereafter the absorbance is measured via plate reader (CYTATON5762 plate reader, Biotek) at 450 nm against a background blank. The reference wavelength is set to 650 nm. Data are expressed as T/C [%] and the graphs are obtained after performance of n=4 biological experiments.

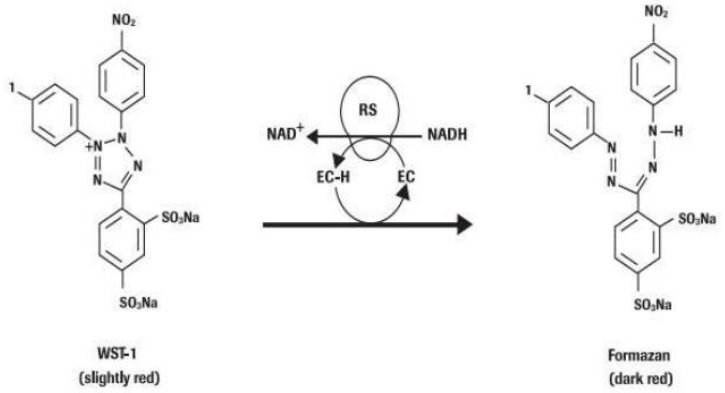

Figure 12: Cleavage of tetrazolium salt WST-1 to formazan

(RS = mitrochondrial succinate-tetrazolium-reductase system, EC = electron coupling reagent). Source: Merck (https://www.merckmillipore.com)

The last replicate was stained using Cell mask™ Deep red plasma membrane. For this procedure the cells are washed twice with LCI and 100 µL of staining solution (Cell mask™ Deep red plasma membrane: LCI, 1:2000) are added to each well. After 15 min incubation at RT, the wells are washed twice with LCI and 200 µL LCI are added to each well before imaging. Images are captured using the Lionheart using the CY5 and phase contrast channels. Intensity is measured for all treatments and conditions.

Membrane Fluidity Assay

This assay involves the application and incubation of pyrene-dodecanoic acid (PDA) which can be biosynthetically incorporated into the cell membrane in sufficient quantities to produce the degree of labelling required for long-wavelength pyrene excimer fluorescence. Depending on the fluidity of the membrane different ratios of monomer and excimer are formed in the membrane leading to an increase or decrease of fluorescence [80, 86].

Prior to carrying out the membrane fluidity assay, the cells of both the HCT116 and HCEC-1CT lines are seeded into a 96-well clear bottom black side plate 48h in advance. After 24h hours the treatment is applied and incubated for 24h at 37°C (5% CO_2).

For the membrane fluidity assay a 10 mM PDA stock solution in DMSO is prepared freshly each time. The stock solution is diluted 1:1000 with Life Cell Imaging Solution (LCI) (for HCT116) or serum free media (for HCEC-1CT colourless DMEM, HEPES, penstrep). The cell

culture medium is aspirated and 100 µL PDA in LCI/media is added to each well. The PDA is incubated for one hour at 37°C (5% CO_2). Thereafter the PDA-LCI/medium solution is removed and 100 µL of stimuli (MßCD 50 µM, MßCD-Chol 10 µM, H_2O_2 1mM) is added to the wells designated as stimuli controls. The wells treated with PA, OA and CER are covered with 100 µL colourless DMEM (HCEC-1CT) or LCI (HCT 116). Then the plate is incubated for 10 min. The fluorescence intensity is measured once using a plate reader. For the monomer the excitation wavelength is 344 nm and the emission 375 nm. For the excimer 344 nm and 470 nm respectively. Data are expressed as intensity [excimer/monomer] and the graphs are obtained after performance of at least n=3 biological experiments.

Immunostaining: Piezo1 Ion Channels, Actin

To carry out the staining of the Piezo1 channels a previously implemented protocol by Del Favero *et al*., 2020 is adapted [87] and 8-well slides for both cell lines are prepared. For the HCEC-1CT the cells are seeded at a concentration of 100 000 cells/mL or 25 000 cells per well (250µL). For the HCT116 the cells are seeded at a concentration of 240 000 cells/mL or 60 000 cells per well (250µL). Two wells act as controls, two wells are treated with palmitic acid (25 or 100µM), two wells are treated with oleic acid (25 or 100µM) and the remaining two wells are treated with a cerulenin concentration of 10µM. Concentrations are chosen on the basis of the outcome of the cytotoxicity and membrane fluidity experiments. Following an incubation time of 24h at 37°C (CO_2 5%) the cells are fixed with formaldehyde (3,7 % in PBS). This is done in the dark for 15min with two washing steps using PBS-A hereafter. The 8-well slides are sealed and stored at 4°C until the staining procedure.

First, a blocking step is made to ensure that unspecific binding sites are blocked. For this 2% donkey serum (Sigma Aldrich) in PBS-A (250µL/well) is applied for 1 hour at room temperature. The blocking mixture is removed and the Piezo1 antibodies are applied at a 1:400 dilution in PBS-A (200µL/well). The antibodies are incubated at 4°C overnight.

On the following day a series of washing steps (3x 10min; 2x 5min) are carried out with PBS-A only. In order to privilege the localization of Piezo1 membrane proteins, this step was performed without detergents.

Next the secondary donkey-anti-rabbit antibodies (Invitrogen – Alexa Fluor™ 568 donkey-anti-rabbit) are added with a dilution of 1:1000 in PBS-A. The secondary antibodies are

incubated for 1,5 h in the dark. Following this the wells are again washed (3x 10min; 2x 5min) with PBS-A only, using the rocking table.

The permeabilization of the cell membrane is achieved by using 0,2 % TritonX-100 in PBS-A and adding 200µL of the mixture to each well for 10min. Hereafter another blocking step is carried out with 2 % donkey serum in PBS-A (250 µL) for 1h at room temperature in the dark.

Next 200µL phalloidin (Invitrogen - Oregon Green® 488 phalloidin) is added with a dilution of 1:500 in PBS-A to each well to stain the cytoskeleton (actin). The phalloidin is incubated at room temperature for 1,5h. After this another series of washing steps are applied: firstly, 3x 10min using the washing buffer Triton-X (0,05 % in PBS-A); secondly, 2x 5min using PBS-A only.

To complete the staining procedure a post fixation step is carried out using 3,5 % formaldehyde in PBS-A. 200µL of the mixture is added to each well and incubated for 10min in the dark. Hereafter each well is washed with 250µL PBS-A and 200µL PBS-glycin is added to inactivate the remaining formaldehyde for 5min using the rocking table. This is removed and another 250µL PBS-A are added to each well.

The PBS-A is removed and 3 – 4 drops of mounting media are applied to each well. The mounting media contains DAPI which stains the nuclei as well as glycerol with serves to keep the air out as well as minimizing the potential photobleaching of the fluorescent molecule. The 8-well slides are sealed with a lid, parafilm and foil and are kept at 4°C for imaging.

Images for Piezo1 (568 nm*), actin (488 nm*) and nuclei (358 nm*) are acquired with LSM Zeiss 710 equipped with ELYRA PS.1 system with a Plan Apochromat 63X/1.4 oil objective (zoom 1.5). At least 3 images are taken from each well and single cell selections are made for at least 5 cells per well. Images are analysed with ZEN 2012 SP3 and FIJI. (* absorption maximum)

Immunostaining:YAP1

To carry out the YAP1 immunostaining again, the previously implemented protocol by Del Favero *et al*., 2020 is adapted [87]. First, pores are created on the cell membrane using the TritonX buffer (= permeabilization buffer; 0,2% TritonX-100 in PBS-A). 200µL of this solution is applied to each well and incubated for 10min at RT. The permeabilization buffer is then

removed and the 250µL of blocking buffer is added to each well. The blocking buffer used is 2% donkey serum in PBS-A. This is incubated for one hour, RT in the dark. The buffer is removed and 200µL of the primary antibody (Rb m Ab to YAP1, Abcam) at a 1:700 dilution in PBS-A is added to each well and incubated overnight at 4°C.

On the following day a series of washing steps is carried out always using the rocking table. Firstly, 250µL of washing buffer consisting of 0,05% TritonX in PBS-A is added to each well. This procedure is carried out 3x10mins. Secondly, 250µL of only PBS-A is added to each well and washed for 3x5mins.

Having removed the PBS-A, 200µL of labelled secondary antibodies (donkey-anti-rabbit, 1:1000 dilution in PBS-A) and phalloidin (1:500 dilution in PBS-A) are added to each well and incubated for 1,5 hours in the dark. Thereafter another series of washing steps are carried out: 3x10mins using the washing buffer and 3x10mins using PBS-A only. Each time 250µL of the solution is added to each well.

For the post fixation the liquid is removed and 200µL 3,7% formaldehyde in PBS-A is added to each well and incubated between 10 – 15 mins, at RT in the dark. The formaldehyde is collected, and the wells washed with 250µL PBS-A, which is also collected with the formaldehyde waste. Hereafter 200µL PBS-glycin is added to each well for 5mins to inactivate any formaldehyde activity. The PBS-glycin is removed and 250µL PBS-A is added to each well, which is again removed. Lastly 3-4 drops of mounting media are added to each well and the plates are sealed and stored at 4°C for further use.

Images for YAP1 (568 nm*), actin (488 nm*) and nuclei (358 nm*) are acquired with LSM Zeiss 710 equipped with ELYRA PS.1 system with a Plan Apochromat 63X/1.4 oil objective (zoom 1.5). At least 3 images are taken from each well and single cell selections are made for at least 5 cells per well. Images are analysed with ZEN 2012 SP3 and FIJI. (* absorption maximum)

Rhodamine-labelled palmitic acid

To carry out the experiment using rhodamine-labelled palmitic acid, 8-well slides for both cell lines are prepared. For the HCEC-1CT the cells are seeded at a concentration of 100 000 cells/mL or 25 000 cells per well (250µL). For the HCT116 the cells are seeded at a concentration of 240 000 cells/mL or 60 000 cells per well (250µL). Four wells act as controls (two 0 % serum; two 10 % serum) the remaining four wells are treated with rhodamine-labelled PA, two with 0 % serum, and two well with 10 % serum. The rhodamine-PA solution is only vortexed and not sonicated as not to break the bond between rhodamine and PA. The treatment is incubated for 24h (37 °C, 5 % CO_2). After incubation the cells are washed and LCI is added to each well before images are captured with LSM Zeiss 710 equipped with ELYRA PS.1 system with a Plan Apochromat 63X/1.4 water objective.

3.2.3 Imaging and Statistical Analysis

Image analysis: Live cell imaging is done using the Lionheart FX automated microscope (BioTek Instruments Inc., Winooski, VT, USA), using the CY5 and phase contrast channels.

Images for Piezo1, actin and YAP1 are acquired with LSM Zeiss 710 (Carl Zeiss AG, Oberkochen, GER) equipped with ELYRA PS.1 system with a Plan Apochromat 63X/1.4 oil objective (zoom 1.5) and an AndoriXon 897 (EMCCD) camera.

Images are analysed with ZEN 2012 SP3 and FIJI. Regions of interest (ROI) are selected and evaluated with the software.

Statistical analysis: Analysis is conducted using Excel and OriginPro® 2022 software. One way ANOVA with Fischer LSD for multiple comparison is performed for all data. Differences were considered significant applying a threshold value (p) of 0.05.

4 Results

4.1 Cytotoxicity

The results of the WST-1 assay are expressed as T/C (test/control) in percent. The controls are set to 100 %, and the percentage of the viable cells for each condition can be determined. The highest concentration tested (500 µM) has a cytotoxic effect for all compounds on both cell lines. CER also has a toxic effect at a concentration of 250 µM. At the concentration of 250 µM, PA also triggers a loss of viable cells. The lower concentrations (PA, OA – 25 µM, 50 µM, 100 µM; CER – 5 µM, 10 µM, 25µM) had no appreciable toxicity or even supported cell proliferation . The purpose of the cytotoxicity assay was to find working concentrations for further experiments in which the cells exhibit no adverse reaction to the compounds.

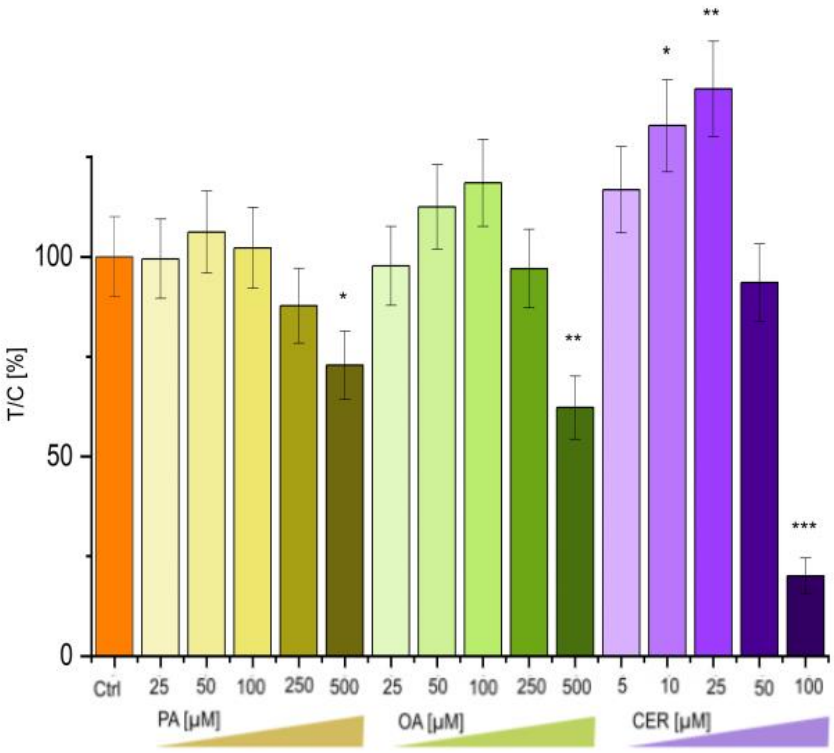

Figure 13: WST-1: Cytotoxicity in the HCT 116 cell line

*Displayed are the means plus standard error of mean for each treatment condition as treatment over control for the HCT 116 cell line. Ctrl = control; yellow green = PA in increasing concentration [µM]; green = OA in increasing concentration [µM]; violet = CER in increasing concentration [µM]; Data are expressed as T/C [%] and obtained after n = 4 biol. experiments. significant difference to control with *p<0,05, **p<0,01, ***p<0.001, all others not significant, error bars: standard error (ANOVA).*

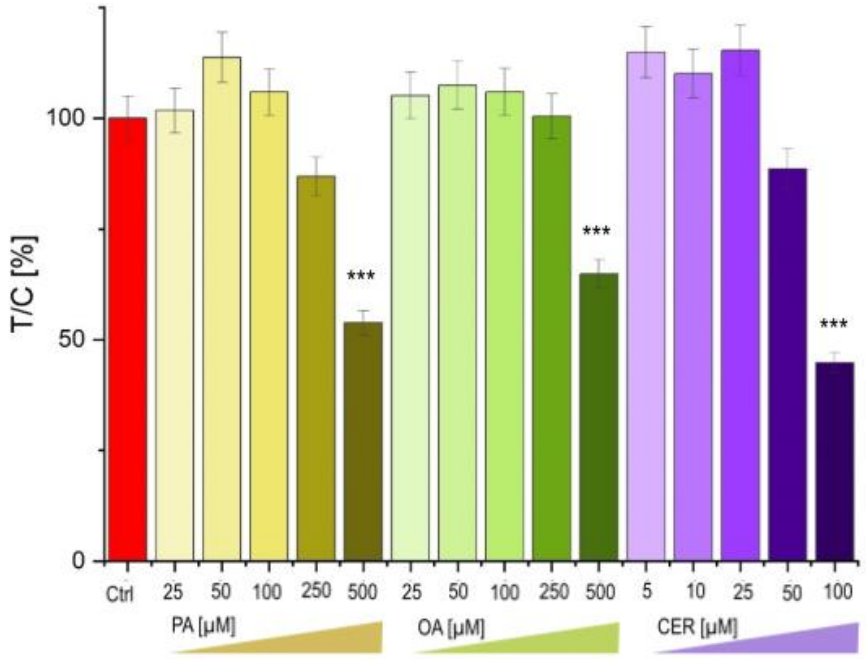

Figure 14: WST-1: Cytotoxicity in the HCEC-1CT cell line

*Displayed are the means plus standard error of mean for each treatment condition as treatment over control for the HCEC-1CT cell line. Ctrl = control; yellow green = PA in increasing concentration [µM]; green = OA in increasing concentration [µM]; violet = CER in increasing concentration [µM]; Data are expressed as T/C [%] and obtained after n = 4 biol. experiments; significant difference to control with ***p<0.001, all others not significant, error bars: standard error (ANOVA).*

The cytotoxic effects can be clearly seen (figures 15 and 16) in the images acquired with the Lionheart FX automated microscope after the staining with Cell mask™ Deep red plasma membrane stain.

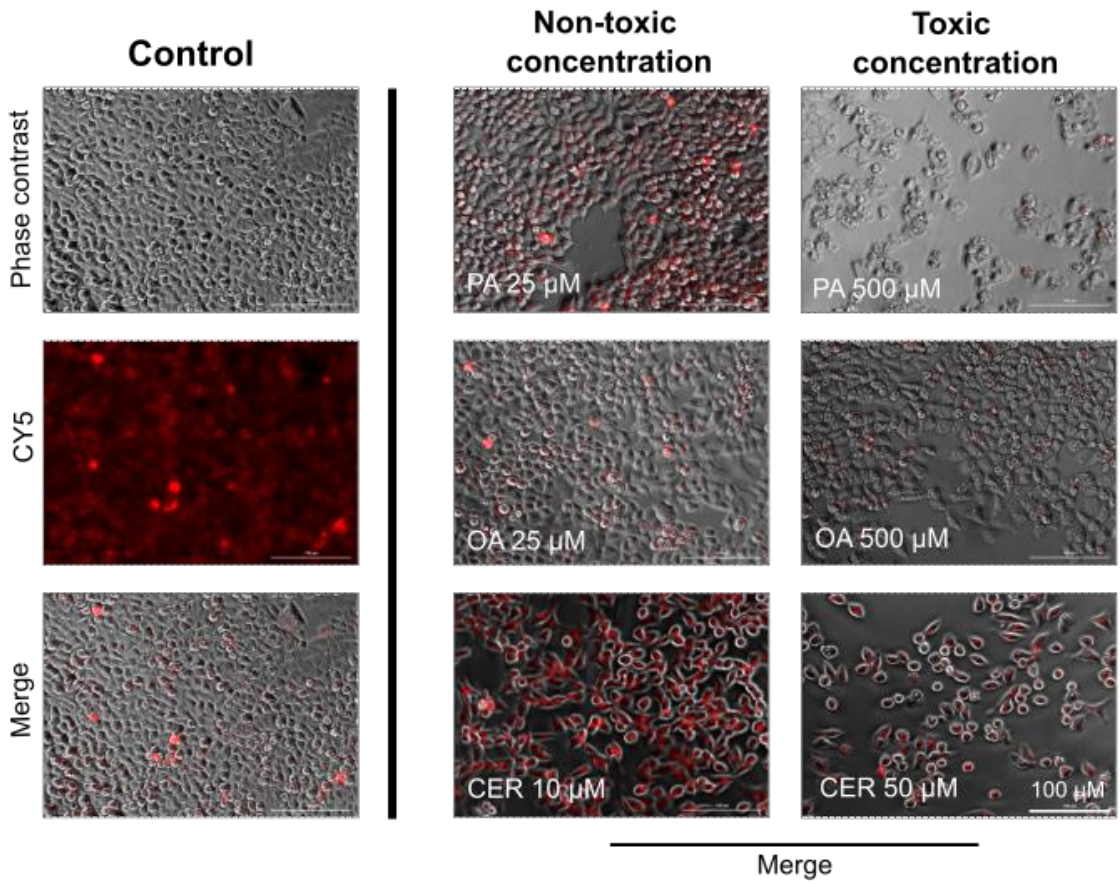

Figure 15: Images of cytotoxicity in HCT 116 cells

Representative images of the appearance of HCT 116 cells after incubation with toxic and non-toxic concentrations of treatments with PA, OA, and CER (all phase contrast and CY5 merge) as compared to control (phase contrast, CY5 and phase contrast and CY5 merge). A decrease in cells' density and change in morphology can be seen for toxic concentrations. The images are acquired with the Lionheart FX automated microscope after staining the cells with Cell mask™ Deep red plasma membrane stain.

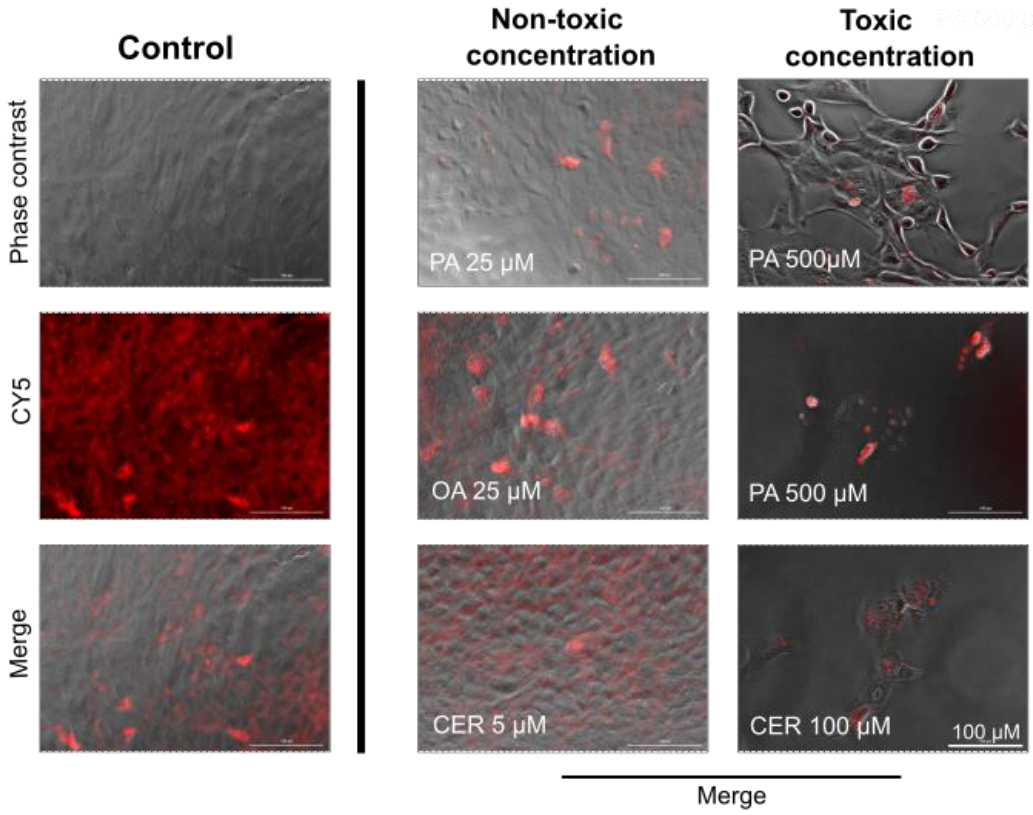

Figure 16: Images of cytotoxicity in HCEC-1CT cells

Representative images of the appearance of HCEC-1CT cells after incubation with toxic and non-toxic concentrations of treatments with PA, OA, and CER (all phase contrast and CY5 merge) as compared to control (phase contrast, CY5 and phase contrast and CY5 merge). A decrease in cells' density and change in morphology can be seen for toxic concentrations. The images are acquired with the Lionheart FX automated microscope after staining the cells with Cell mask™ Deep red plasma membrane stain.

4.2 Membrane Fluidity

When comparing controls of both cell lines with one another it can be observed, that the HCT116 cell line is less fluid than the HCEC-1CT. The cancer cells exhibit a significant ($p < 0{,}001$) decrease in membrane fluidity with an increase of the concentration (25 µM, 50 µM, 100 µM) for both PA and OA and at 250 µM (OA) (figure 17, 1a and 1b). The relative increase in fluidity for the treatment with PA (250 µM, 500 µM) and OA (250 µM) is more likely due to the cytotoxic effect as demonstrated in the WST-1 assay results and in the bright filed images

(figures 13 - 16). Here the dying cells lose the integrity of the plasma membrane and are able to incorporate more PDA forming more excimers resulting in a higher signal. This effect is even more pronounced in the highest concentration for both PA and OA in the HCEC-1CT cells. Otherwise only the treatment with 100 µM PA resulted in a significant ($p < 0{,}001$) decrease in cell membrane fluidity in the HCEC-1CT cell line (figure 17, 2a).

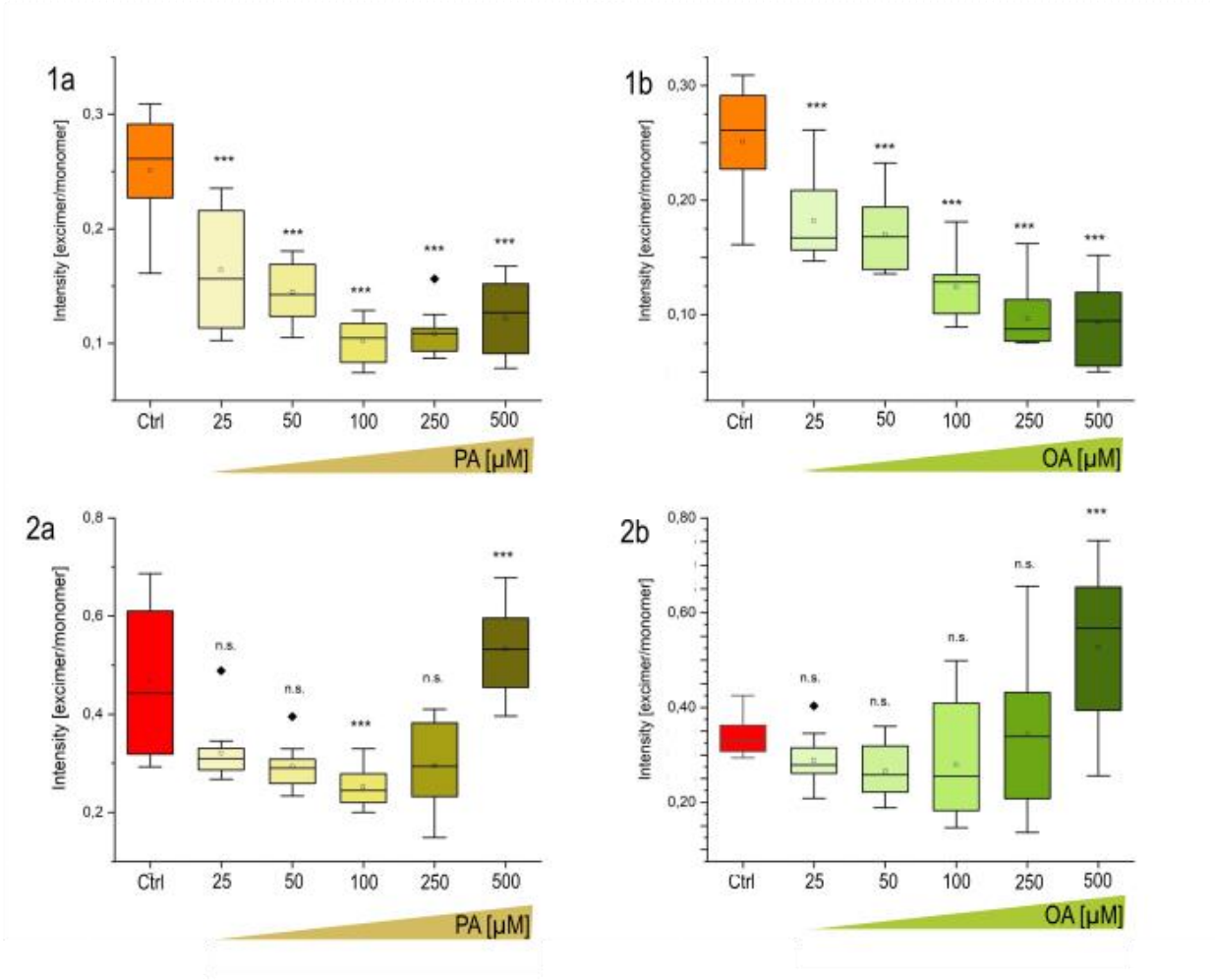

Figure 17: Effect of PA and OA on Membrane fluidity

The data of the membrane fluidity assay are expressed as intensity [excimer/monomer]. Graphs 1a and 1b represent the cancer cell line HCT 116, with 1a representing the significant decrease in membrane fluidity after treatment with different concentrations of PA depicted in yellow green in [µM] (24 h) and 1b representing the significant decrease in membrane fluidity after treatment with different concentrations of OA depicted in green in [µM] (24 h). HCT 116 controls are orange. Graphs 2a and 2b represent the non-tumorigenic intestinal cell line HCEC-1CT, with 2a representing the change in membrane fluidity after treatment with different concentrations of PA depicted in yellow green in [µM] (24 h) and 1b representing no change (with exception of 500 µM) in membrane fluidity after treatment

*with different concentrations of OA depicted in green in [µM] (24 h). HCEC-1CT controls are red. Error bars: standard error; boxes: 25/75 percentile with mean. Data are obtained after at least n = 3 biological replicates. Significant difference to control with ***p<0.001, n.s.= no significance (ANOVA).*

4.3 Piezo1 Ion Channels

Due to changes in membrane fluidity it was expected that a change in Piezo1 ion channels would be seen in the cell membrane, however in general the change was not significant for the treatment with fatty acids (figure 18 and 19). Only in the HCT116 cell line the treatment with PA (100 µM) led to an increase in the expression of Piezo1 ion channels (figure 18). Cerulenin on the other hand, had opposing effects on the expression of Piezo1 in the different cell lines; a significant (p<0,01) increase in HCT116 and a significant (p<0,001) decrease in HCEC-1CT (figure 20).

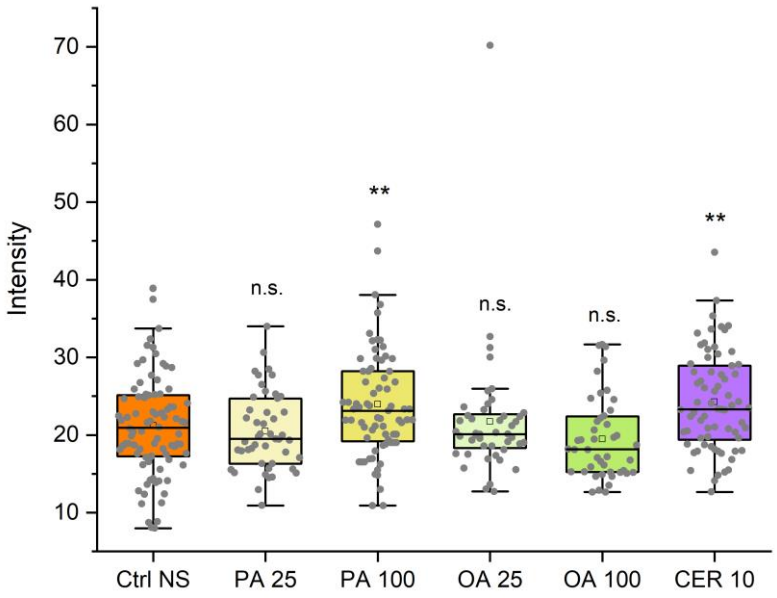

Figure 18: Piezo1 expression in the HCT 116 cell line

*In the HCT 116 cell line only the treatment with 100 µM PA (24 h) and 10 µM CER (24 h) led to a significant increase of Piezo1. Other treatments with PA and OA had no effect on Piezo1 expression. Data are expressed as intensity at 568 nm and the graphs are obtained after performance of at least n=3 biol. replicates in techn. n=major of 360 cells/ROIs; Significant difference to control with **p<0.01, n.s. = no significance; Error bars: standard error; boxes: 25/75 percentile with mean (ANOVA).*

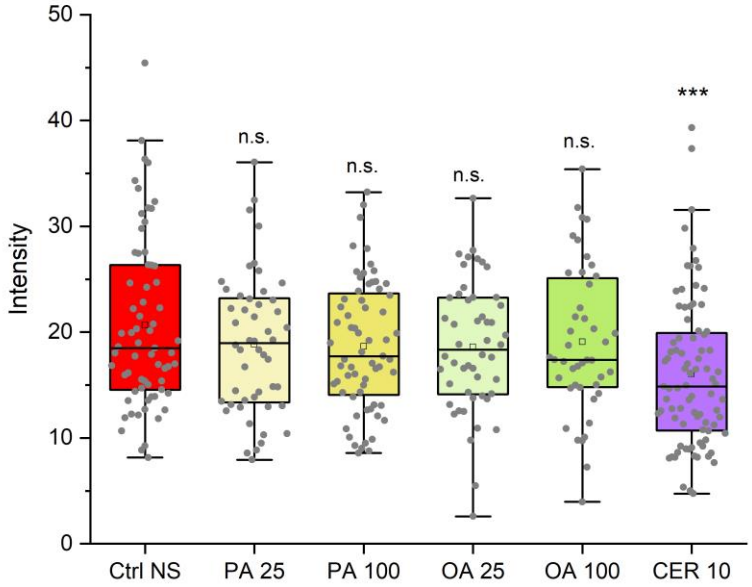

Figure 19: Piezo1 expression in the HCE-1CT cell line

*In the HCEC-1CT cell line only the treatment with 10 µM CER (24 h) led to a significant decrease of Piezo1. Treatments with PA and OA had no effect on Piezo1 expression. Data are expressed as intensity at 568 nm and the graphs are obtained after performance of at least n=3 biol. replicates in techn. n=major of 360 cells/ROIs; Significant difference to control with ***p<0.001, n.s. = no significance; Error bars: standard error; boxes: 25/75 percentile with mean (ANOVA).*

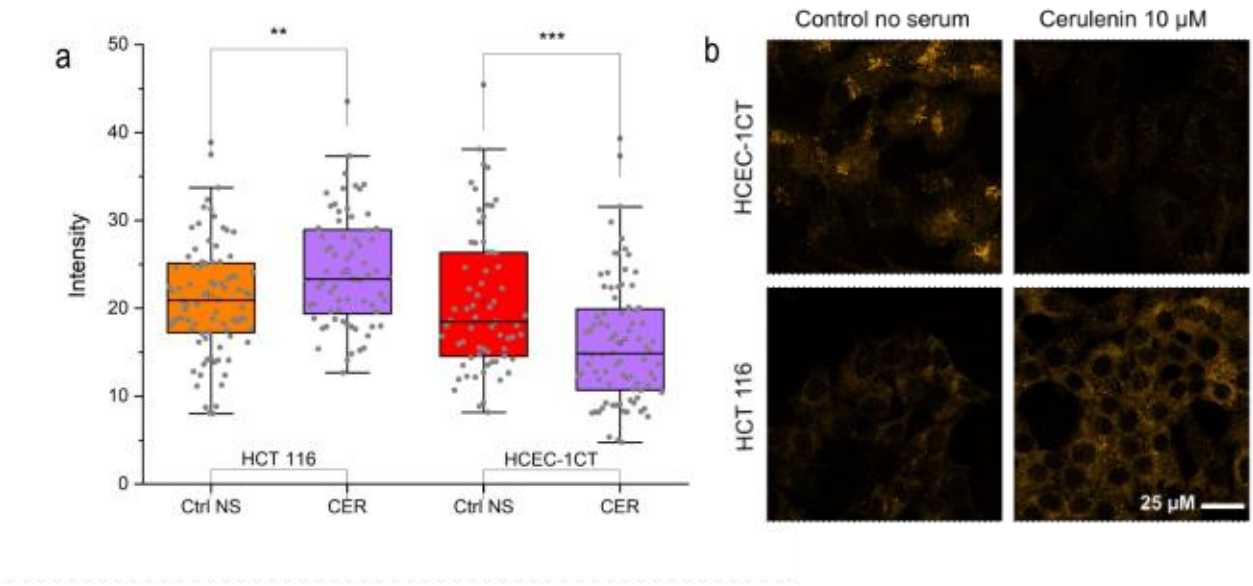

Figure 20: Comparison of Piezo1 expression in both cell lines after treatment with cerulenin

a: *Treatment with CER (violet, 10 µM, 24h) had opposing effects on the two cell lines. This is an indication of the difference in lipid metabolism in cancer (orange) and non-tumorigenic cells (red) affecting the mechanodransductory apparatus of the intestine. Data are expressed as intensity at 568 nm and the graphs are obtained after performance of at least n=3 biol. replicates in techn. n=major of 60 cells/ROIs (one grey dot = one cell/ROI) for each condition; significant difference to control (Ctrl NS = control no serum) with **p<0.01, ***p<0.001; error bars: standard error; boxes: 25/75 percentile with mean. (ANOVA).* ***b:*** *The decrease of the expression of Piezo1in the HCEC-1CT cell line and the increase of Piezo1 in the HCT 116 cell line after treatment with CER (10 µm, 24 h) can be observed (immunostaining, Piezo1 shown in orange). Images acquired at 568 nm with LSM Zeiss 710 equipped with ELYRA PS.1 system with a Plan Apochromat 63X/1.4 oil objective.*

4.4 Actin

Looking for additional components of the cell mechanosensory apparatus we decided to verify the effects of our cells on actin cytoskeleton. In the tumorigenic cell line, collectively a significant (p<0,001) increase of actin could be observed for all treatments and concentrations compared to controls (figure 21). Sharper concentration dependent responses could be identified in the HCEC-1CT cell line. Ranging from no significance (OA, 25 µM), over a significant (p<0,05, PA, 25 µM), to a highly significant (p<0,001, PA 100 µM, OA 100 µM, CER 10 µM) increase in actin compared to controls (figure 22). Images of actin were captured with the LSM Zeiss 710 after staining actin with phalloidin. The changes in actin after treatment

with PA and OA can be viewed in figure 23, with only actin and as merge (Piezo1, actin & DAPI).

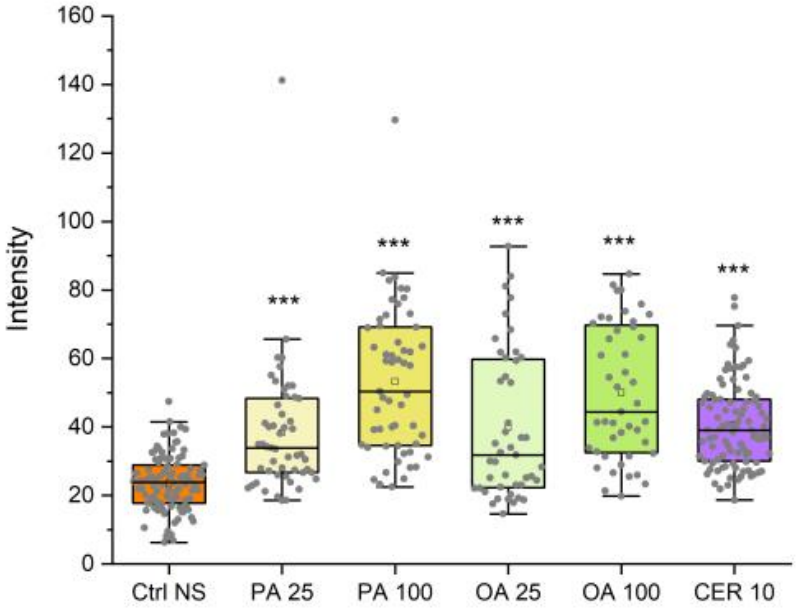

Figure 21: Significant increase of actin after treatment with PA, OA and CER in HCT 116

*A significant (p<0,001) increase in actin is observed for all concentrations and compounds (PA (yellow) 25 µM, 100 µM; OA (green) 25 µM, 100 µM; CER (violet) 10 µM) in the cancer cell line HCT 116 compared to no serum controls (orange). Data are expressed as intensity at 488 nm and the graphs are obtained after performance of at least n=3 biol. replicates in techn. n=major of 390 cells/ROIs (one grey dot = one cell/ROI); significant difference to control with ***p<0.001; error bars: standard error; boxes: 25/75 percentile with mean (ANOVA).*

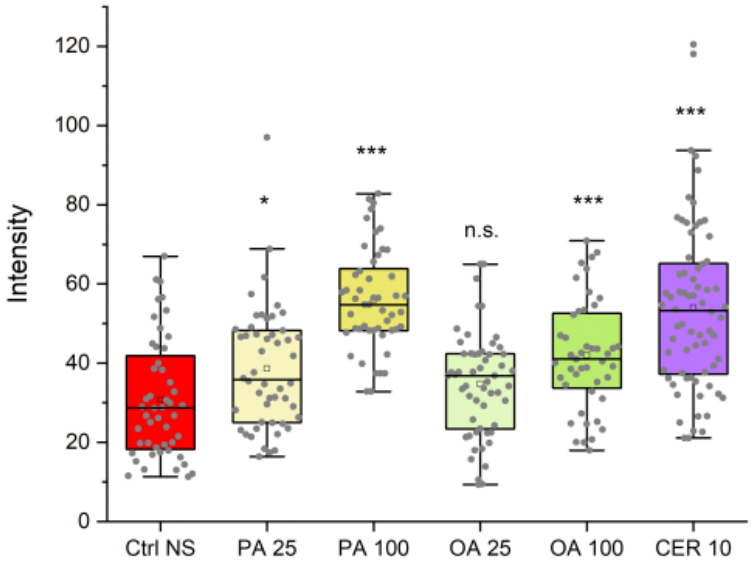

Figure 22: Change of actin in the HCEC-1CT cell line after treatment with PA, OA and CER

*A variety of effects on actin is observed the HCEC-1CT cell line. No significant difference is observed for treatment with 25 µM OA. A significant increase for all remaining concentrations and compounds (PA (yellow) 25 µM, 100 µM; OA (green) 100 µM; CER (violet) 10 µM) is seen compared to no serum controls (red). Data are expressed as intensity at 488 nm and the graphs are obtained after performance of at least n=3 biol. replicates in techn. n=major of 345 cells/ROIs (one grey dot = one cell/ROI); significant difference to control with *p<0,05, ***p<0.001, n.s. = no significance; error bars: standard error; boxes: 25/75 percentile with mean (ANOVA).*

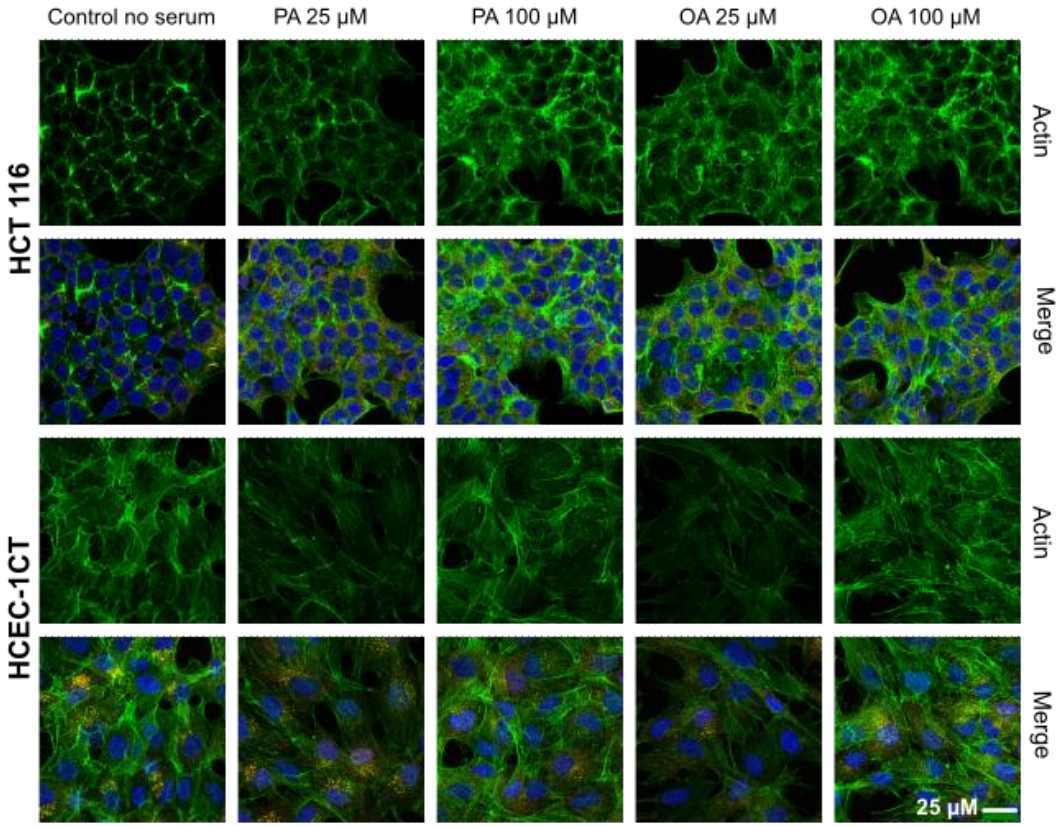

Figure 23: Images of actin stained by phalloidin in both intestinal cell lines

Actin (green) distribution in the HCT 116 and HCEC-1CT cell line. In the HCT 116 cells the more intense colouring of actin (stained with phalloidin) of the treated cells can be seen when compared to controls corresponding to the data in figure 21. A variation of intensity of actin can be seen in the HCEC-1CT cells (see also figure 22). Depicted above are also merged images of actin (488 nm, green), Piezo1 (568 nm, orange) and nuclei (358 nm, blue). Images are acquired with LSM Zeiss 710 equipped with ELYRA PS.1 system with a Plan Apochromat 63X/1.4 oil objective.

4.5 YAP1

After observing a significant change in actin cytoskeleton, we pursued the hypothesis that mechanosensitive transcription factors could change their localization profile upon incubation with the fatty acids. An increase in YAP1 in the nucleus corresponds potentially to an increase in the activity as a transcription factor. When comparing controls of both cell lines there are overall higher levels of YAP1 in both the cytosol and the nucleus of the HCEC-1CT cell line, and lower levels in HCT116 cells (figure 24 a-c). Furthermore, in both cell lines and all

conditions it could be observed that levels of YAP1 are higher in the nucleus than in the cytosol, though to different degrees (figure 25 a and b).

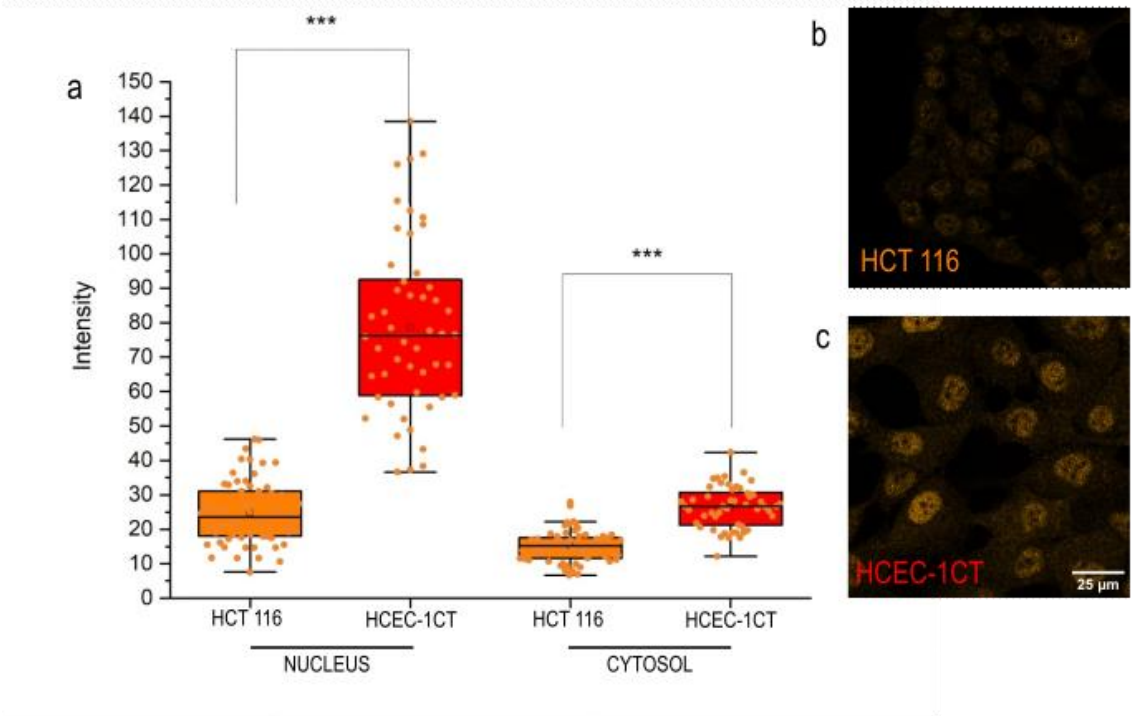

Figure 24: Comparison of controls of both cell lines in regard to YAP1 expression

Of notice the significant (p<0,001) difference in YAP1 expression in both the nucleus and cytosol for both cell lines: ***a:*** *YAP1 expression is higher in the HCEC-1CT (red) cell line in both the nucleus and cytosol when compared to the HCT 116 (orange) cell line. Data are expressed as intensity at 568 nm and the graphs are obtained after performance of at least n=3 biol. replicates in techn. n=major of 220 cells/ROIs (one grey dot = one cell/ROI); significant difference to control with *p<0,05, ***p<0.001, n.s. = no significance; error bars: standard error; boxes: 25/75 percentile with mean (ANOVA).* ***b:*** *Image depicting YAP1 expression in the cancer cell line.* ***c:*** *Image depicting YAP1 expression in the non-tumorigenic cell line. Here the higher concentration of YAP1 in the nucleus can be observed in comparison to the cytosol. Furthermore, the higher intensity when compared to "b" can clearly be seen, reflecting on the data in "a". Images are acquired at 568 nm with the LSM Zeiss 710 equipped with ELYRA PS.1 system with a Plan Apochromat 63X/1.4 oil objective.*

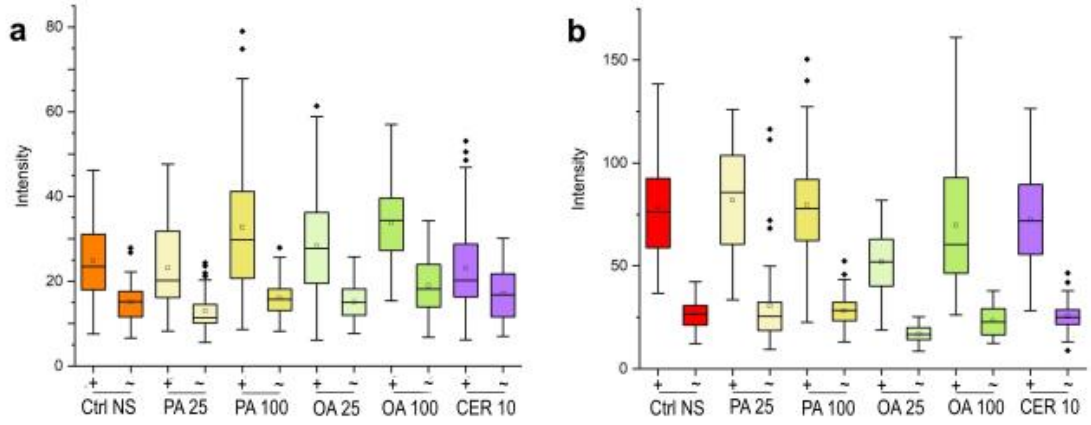

Figure 25: An overview of YAP1 expression in both cell lines and all treatments

An overview of the data on the expression of YAP1 in both cell lines shows that the expression of YAP1 is higher in the nucleus (+ = nucleus) for all treatments and conditions when compared to YAP1 expression in the cytosol (~ = cytosol). Quantification and experimental details are shown in figures 26 and 28. ***a****: The intensity for YAP1 measured at 568 nm is at a lower range (approx. between 10 to 45) in the HCT 116 cell line than in the non-tumorigenic cell line (b). Concentrations are expressed in [µM], no serum controls (orange), PA (yellow), OA (green), CER (violet).* ***b:*** *The intensity of YAP1 ranges between approx. 30 and 110 measured at 568 nm in the HCEC-1CT cell line. Concentrations are expressed in [µM], no serum controls (red), PA (yellow), OA (green), CER (violet).*

With respect to YAP1 in the nucleus following observations were made: The presence of cerulenin induced no change in HCT116. However the treatment with fatty acids has divergent effects. The high concentration (100 µM) of both PA and OA increases the amount YAP1 in the nucleus significantly ($p<0,001$), whereas a low concentration (25 µM) of PA leads to a significant ($p<0,001$) decrease and a low concentration (25 µM) of OA conversely leads to an increase ($p<0,05$) in YAP1.

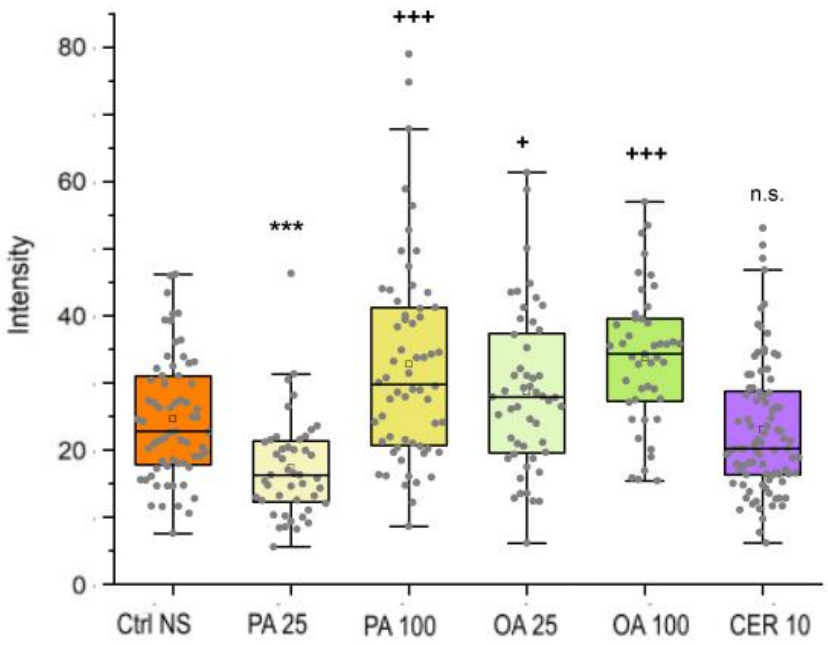

Figure 26: YAP1 expression in the nucleus of HCT 116 cells

*The treatments had a variety of effects on YAP1 expression in the nucleus. Compared to the no serum controls (orange) there is a significant increase in YAP1 after treatment (24 h) with PA (100 µM, yellow), OA (25 µM, 100 µM, green) and a significant decrease with PA 25 µM. Treatment with CER (10 µM, violet) led to no significant difference. Data are expressed as intensity at 568 nm and the graphs are obtained after performance of at least n=3 biol. replicates in techn. n=major of 350 cells/ROIs (one grey dot = one cell/ROI); significant difference to control with +p<0,05, +++p<0.001, ***p<0,001, n.s. = no significance; error bars: standard error; boxes: 25/75 percentile with mean (ANOVA).*

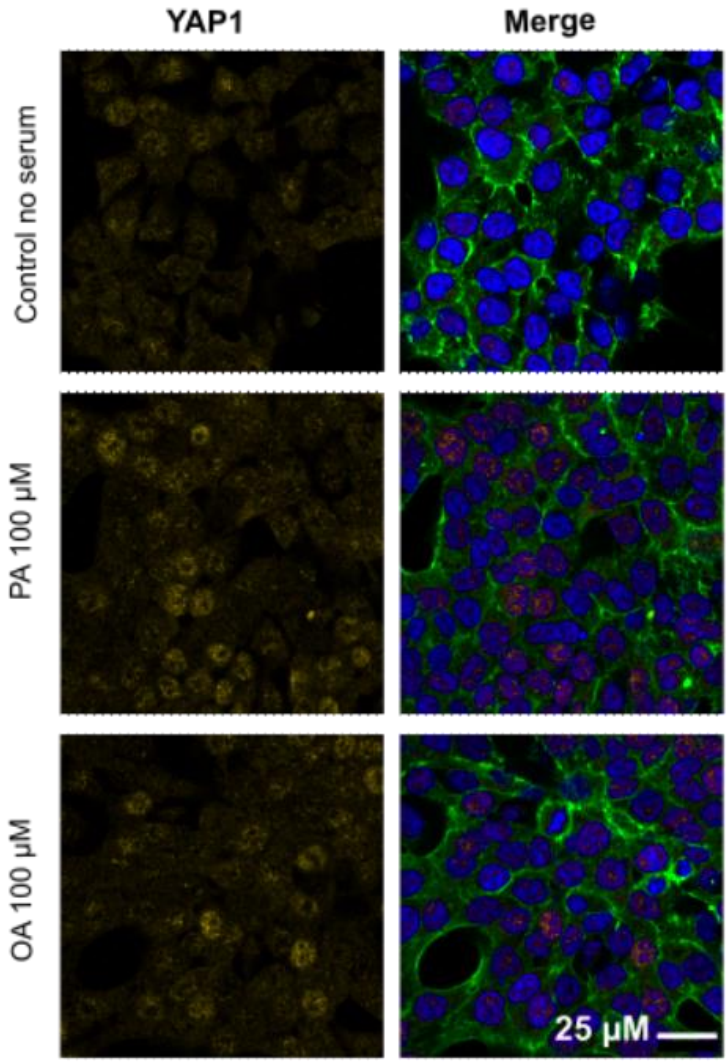

Figure 27: Images of YAP1 expression in HCT 116 cells

The difference in intensity of YAP1 can be clearly seen in the treatment of the cells with 100 µM PA and 100 µM OA in comparison to the control (further treatments are not depicted, but data can be obtained in figure 26). Both treatments led to a significant ($p<0,001$) increase of YAP1 expression in the nucleus. Depicted above are also merged images of YAP1 (568 nm, orange), actin (488 nm, green), and nuclei (358 nm, blue). Images are acquired with the LSM Zeiss 710 equipped with ELYRA PS.1 system with a Plan Apochromat 63X/1.4 oil objective.

In the HCEC-1CT cell line there was no significant difference between the control and all conditions, with exception of a significant (p<0,001) decrease of YAP1 after incubating with 25 µM OA (figure 28). This effect can be clearly seen in the change the intensity of YAP1 (with and without treatment with 25 µM OA) in the images aquired with the LSM (figure 29). Likewise, this is the only treatment which led to no significant difference in regard to actin in HCEC-1CT.

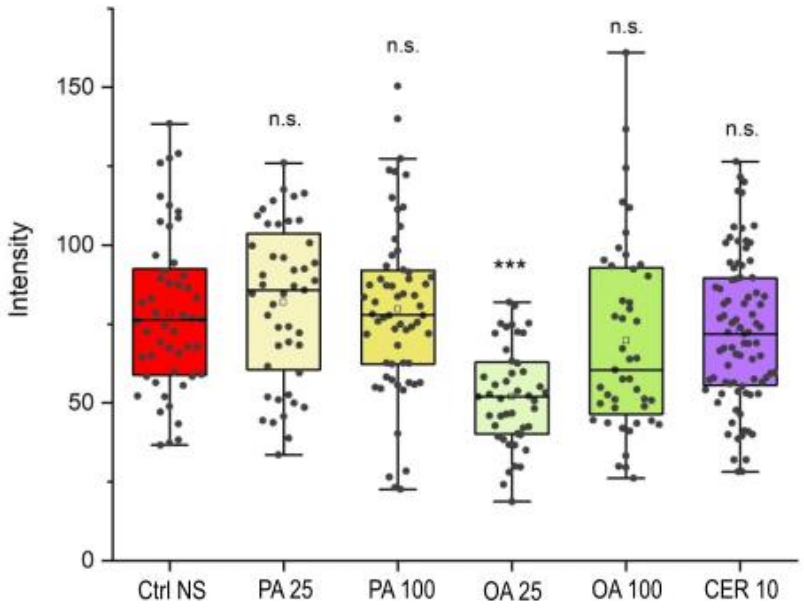

Figure 28: YAP1 expression in the nucleus of HCEC-1CT cells

*Only treatment with OA (25 µM, 24 h, green) led to a significant p<0,001 decrease of YAP1 expression in the nucleus when compared to the control (red). All other treatments and conditions had no effect (PA 25 and 100 µM, green; OA 100 µM, yellow; CER 10 µM, violet). Data are expressed as intensity at 568 nm and the graphs are obtained after performance of at least n=3 biol. replicates in techn. n=major of 330 cells/ROIs (one grey dot = one cell/ROI); significant difference to control with ***p<0.001, n.s. = no significance; error bars: standard error; boxes: 25/75 percentile with mean (ANOVA).*

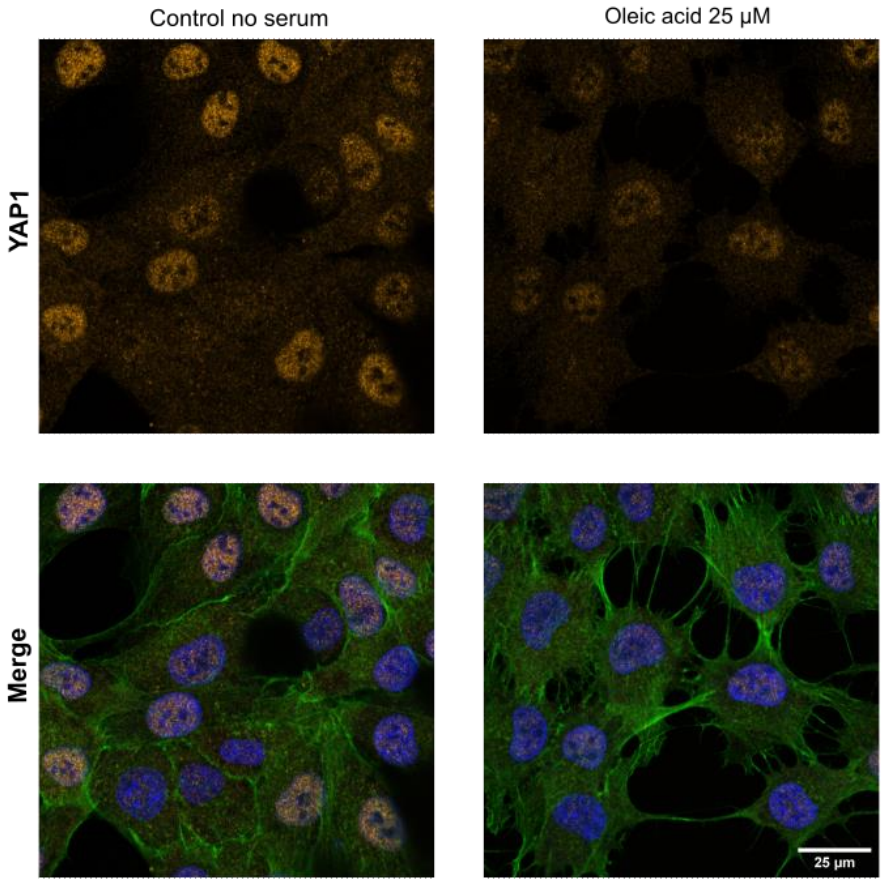

Figure 29: YAP1: Images of treatment with 25 µM OA in HCEC-1CT cells

Only treatment with OA (25 µM, 24 h) led to a significant p<0,001 decrease of YAP1 expression in the nucleus when compared to the control. Above the decrease of the intensity of YAP1 in the OA treated cells can observed, with the controls appearing much brighter. Depicted above are also merged images of YAP1 (568 nm, orange), actin (488 nm, green), and nuclei (358 nm, blue). Images are acquired with the LSM Zeiss 710 equipped with ELYRA PS.1 system with a Plan Apochromat 63X/1.4 oil objective.

4.6 Rhodamine-labelled Palmitic Acid

On the basis of the data at hand, we postulated that the two cell lines could differ in the efficiency to take up the fatty acids. To this aim we performed live-cell imaging experiments with fluorescently labelled PA to observe in detail the intracellular distribution of the compound. Though the analysis of the experiments carried out using rhodamine-labelled PA is foreseen beyond the conclusion of this master thesis, a brief qualitative comparison between the two cell lines can be made. As seen in figure 30 it can be observed that PA incorporates into

the cell membrane of HCT 116 cells as opposed to the HCEC-1CT cell which take PA up into the cells but not into the cell membrane. The uptake was verified by 3D imaging to ensure that PA is within the cell and not on the outside. Here the entirely different uptake of PA in cancer cells and non-tumorigenic cells can be seen as well as dependency on the serum used for the incubation conditions.

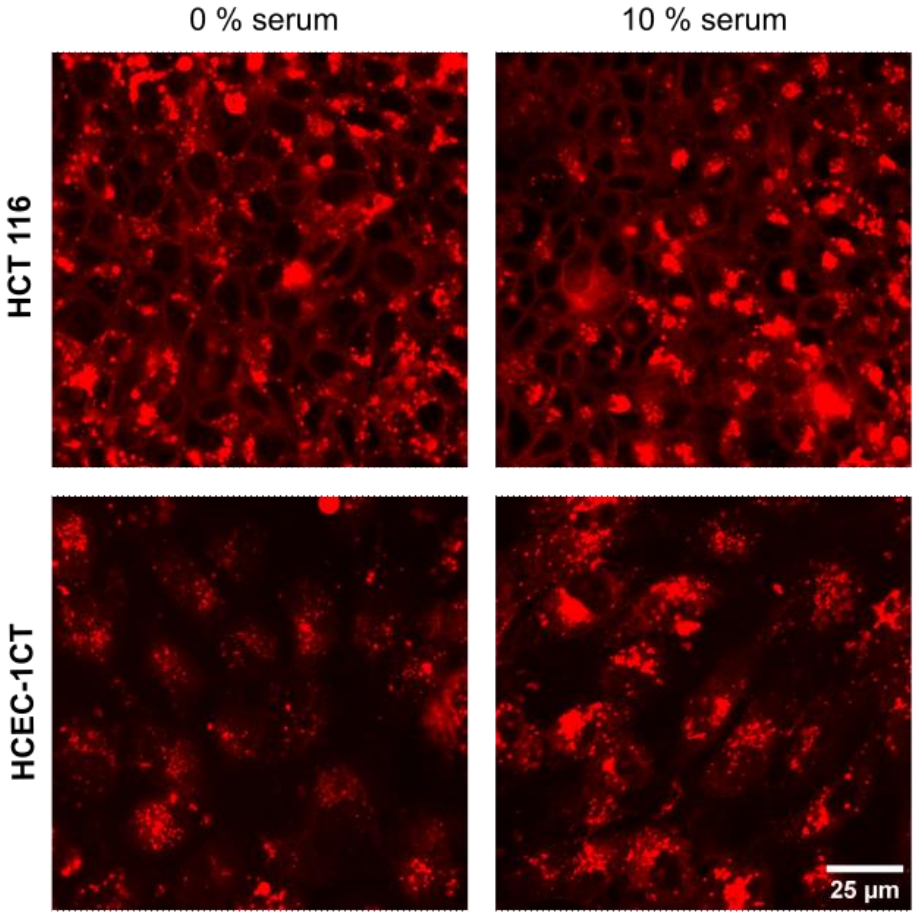

Figure 30: Treatment of both cell lines with rhodamine labelled palmitic acid

On the left, the cells are treated in serum free medium, 25 µM PA; on the right with 10 % serum, 25 µM PA. Different uptake of PA can be observed for both cell lines. HCT 116 cells take up PA into the membrane and the cell. The outline of the cells can be clearly defined. The outline of the HCEC-1CT cells cannot be established, but through 3-D imaging the uptake into the cell could be verified. Images are acquired with the LSM Zeiss 710 equipped with ELYRA PS.1 system with a Plan Apochromat 63X/1.4 water objective.

5 Discussion

It was to be elucidated whether the fatty acids PA and OA have an influence on the mechanosensory apparatus, comparing a cancer cell line to a non-tumorigenic line. Changes in membrane fluidity, Piezo1, actin and YAP1 were assessed and compared to controls and cerulenin treated cells. In the following, results of the experimental work for this thesis will be discussed.

Based on the "force from lipids" principle [12] it stood to test whether PA and OA would induce changes in the rigidity or fluidity of the membrane, which in turn could potentially affect the mechanical properties of the membrane. Recently, research was conducted on the potential effects on membrane fluidity on the mechanosensitive Piezo1 ion channel, by treating mouse neuro-2a (N2A) and human embryonic kidney (HEK) cells with different fatty acids. These included margaric acid (MA, C17:0), and PUFAs such as arachidonic acid (AA, C20:4), eicosapentaenoic acid (EPA, C20:5) and docosahexaenoic acid (DHA, C22:6). Through atomic force microscopy (AFM) and differential scanning calorimetry (DSC) it was determined that membranes containing MA display a higher bending stiffness and are more rigid than those enriched in PUFAs [88]. Based on these results, it was anticipated that like MA, PA belonging to the group of saturated fatty acids would decrease membrane fluidity and OA acid might increase the fluidity slightly due to its only double bond or have no effect due to the shorter chain length when compared to PUFAs. However, the results of the membrane fluidity assay only partly coincided with the expectations. Compared to the controls, both PA and OA treatment for all concentrations (25, 50, 100, 250 and 500 µM) led to a significant ($p<0,001$) decrease of membrane fluidity for the HCT 116 cell line (figure 17 1a and 1b). Surprisingly, both PA and OA did not have this effect on the HCEC-1CT cell line. Only the treatment with 100 µM PA led to a significant ($p<0,001$) decrease compared to the controls (figure 17 2a and 2b). The significant increase in membrane fluidity with the treatment of 500 µM PA (increase after initial decrease in lower concentrations) and 500 µM OA, can be attributed to the cell membrane disintegrating, but also cells losing adhesion and shape, so that they fold on each other. This is due to the cytotoxic effect which could potentially alter the distribution of the PDA and not to a more fluid membrane *per se*. These results however contradict the findings that tumour cells often possess higher membrane fluidity than non-tumour cells. The higher fluidity being a feature that promotes malignancy for example in lung cancer cells [89]. In this respect, it is worth mentioning that cancer cells like HCT 116 divide rapidly. To facilitate

constant cell division, the cell membrane must accommodate accordingly, whereas non-tumorigenic cells like HCEC-1CT exhibit a slower rate of turn-over [90]. However, changes in fluidity could also be transitionary since only one time point (24h) was measured. These results beg the question how dissimilarly the uptake of the fatty acids into the cell membrane is, when comparing the cell lines to each other. Therefore, rhodamine-labelled PA was used to be able to establish whether PA is incorporated into the cell membrane or taken up into the cell to better understand the membrane fluidity results. Though the experiment has not yet been quantified, the qualitative images derived from the experiment clearly demonstrate that PA is indeed incorporated into the cell membrane and taken up in aggregates into the cytoplasm of the HCT 116 cell line. In figure 30 the outline of each cell can be seen, indicating the incorporation into the membrane, as well as PA aggregates within the cells. The HCEC-1CT cell line on the contrary exhibited practically no uptake into the cell membrane, but uptake of PA into the cell in form of tiny droplets. Also, in figure 30 the uptake into the cell (verified by 3-D imaging) can be seen, but essentially no colouring from rhodamine in the cell membrane can be observed, coinciding with the results of the membrane fluidity assay.

In general, the treatment with PA and OA did not lead to an increase or decrease of Piezo1 in the cell membrane. With the exception of the application of 100 µM PA in the HCT 116 cell line, which led to a significant ($p<0,01$) increase of Piezo1, all other treatments with fatty acids led to no significant change (figures 18 and 19). Recently it was demonstrated that an increase of cholesterol led to an increase of Piezo1 incorporated into the membrane [91]. Together with sterols such as cholesterol - gangliosides, and certain glycosphingolipids form microdomains referred to as membrane/lipid rafts (MLR). These regions can either be morphologically apparent invaginations or planar areas. The MLR function as scaffolds for signalling receptors and ion channels, forming clusters of more active signalling platforms which are dependent on interactions with and dynamic rearrangement of the cytoskeleton for their organization [92]. Since Piezo1 are very large ion channels, which have the size of approximately 2500 amino acids with multiple transmembrane regions [45] they might be incorporated into MLR more easily than other regions of the cell membrane. That said, PA and OA possibly do not contribute to the structural rearrangement of the MLR in which large ion channels involved in signalling reside, but rather integrate into regions of the cell membrane that are more uniform and more likely resemble the lipid-bilayer model originally proposed by Singer-Nicolson [27]. Furthermore, the results of the immunostaining *de facto* only account for the Piezo1 ion

channels present in the cell membrane, but not for their functionality. This would have to be determined by further experiments such as Ca^{2+} measurements.

Interestingly, cerulenin had opposing effects on the expression of Piezo1in both cell lines; a significant ($p<0,01$) increase in HCT116 and a significant ($p<0,001$) decrease in HCEC-1CT (figure 20). This is an indication that cancer and non-tumorigenic cells have entirely different lipid management capacity, which in turn reflects on the mechanosensory apparatus of the cells. Cerulenin inhibits the function of FASN. FASN is a multi-enzyme complex which catalyses fatty acid synthesis. The primary function is to catalyse the production of PA from Acetyl-CoA and Malonyl-CoA in the presence of NADPH. The multi-enzyme protein consists of two identical subunits with four C-terminal catalytic domains (thioesterase, acyl carrier protein, enoyl reductase, ketoacyl reductase) and three catalytic domains (ketoacyl synthase, malonyl/acetyltransferase, dehydrase) in the N-terminal region [93, 94]. Cerulenin blocks interaction of malonyl-CoA with FASN by binding to the ß-keto-acyl-ACP synthase moiety. Cerulenin has also shown to stimulate fatty acid oxidation by activating carnitine palmitoyltransferase 1 (CPT1), which is inhibited by malonyl-CoA [77]. FASN is overexpressed in many cancers, including colon cancer, since an increase in *de novo* fatty acids biogenesis is a metabolic trait that equip tumours with survival benefits and proliferative advantages [95]. Therefore, through the inhibition of FASN the metabolic effect is much greater in cancer than in non-cancer cells, which are not as relient on FASN. Cerulenin has been shown to induce apoptosis in the HCT 116 cell line as the treatment was associated with reduced levels of phosphorylated Akt and the activation of p38, inducing caspase-3 cleavage leading to apoptosis [96, 97]. This effect can be seen in the WST-1 assay readout, when comparing HCT 116 cells to HCEC-1CT cells. In figures 13 and 14 a much higher toxic effect of cerulenin (less than 20 % viability) can be observed in the highest concentration (100 µM) on the cancer cells vs. the non-tumorigenic cells. It has been proposed that cell death potentially could stem from the toxic accumulation of malonyl-CoA and not from a lack of fatty acids [98]. Therefore, further experiments with simultaneous treatment of fatty acids with cerulenin could be carried out on the cells to elucidate combinatory effects.

There is an ongoing dynamic interplay between the MLR and the underlying cytoskeleton, which regulates many aspects in the functionality of eukaryotic cells in terms of their adaption to changing environments [92]. A change of actin in the cytoskeleton was observed upon treatment with PA, OA, and CER in both cell lines. When compared to the controls all compounds and concentrations in the HCT 116 cell line showed a significant ($p<0,001$) increase

of actin (figure 21). In the HCEC-1CT cells (figure 22) there was no change after the treatment with 25 µM OA, but a significant increase after the application of PA (25 µM, $p<0,01$; 100 µM, $p<0,001$), OA 100 µM ($p<0,001$) and CER (10 µM, $p<0,001$). This increase can be observed in the images obtained from the LSM after staining actin with phalloidin (figure 23). Since a significant change in the cytoskeleton was observed, it was hypothesized that mechanosensitive transcription factors could potentially be translocated into the nucleus after incubation with PA and OA. Therefore, the transcription factor YAP1 was chosen for further experiments.

YAP/TAZ is connected the Wnt pathway which plays an important role in the intestine. At the core of the canonical Wnt pathway is a multiprotein machinery called destruction complex. When the Wnt pathway is in an "Wnt OFF" state, both ß-catenin and YAP/TAZ associate with Axin and are incorporated into the destruction complex. Phosphorylation prevents YAP/TAZ and ß-catenin from detaching and/or degrading in the cytoplasm. In the "Wnt ON" state the destruction complex is dissembled by Wnt ligands and consequentially the cytosolic inhibition of YAP/TAZ and ß-catenin are abolished, triggering nuclear accumulation and activation of transcriptional responses in the nucleus [56]. The Wnt pathway is crucial for the homeostasis of intestinal stem cells. This is applicable for both crypt homeostasis and stem cell maintenance that rely on active Wnt signalling. Research has verified this using Wnt agonists in transgenic mice which led to the progressive loss of intestinal crypts [99]. When intestinal tissue is damaged, it has the remarkable feature of being able to regenerate. The regenerative process after damage involves a temporary expanded gradient of cell proliferation along the crypt villus axis [100], induced by Wnt/ß-catenin signalling, Sox9, and Myc. Alongside these contributors of regeneration, additional signalling proteins such as YAP1, Src kinase and focal adhesion kinase (FAK) are specifically required [101]. Recent research has demonstrated that the Wnt pathway primes the intestinal crypt for regeneration by activating a gradient of YAP1, TEAD1/2/4 and CD44, which in turn recruits Src. Therefore, to increase cell proliferation and promote regeneration in damaged tissue through YAP-TEAD-mediated transcription, strong Src activation and consequent translocation of YAP to the nucleus are essential. There exists a synergism between YAP and Wnt signalling which is necessary for amplification of Myc and Sox9 expression domain in the regenerating crypt. After approximately a week the crypt returns to its homeostatic state through a negative feedback process which reduces Wnt signalling [101].

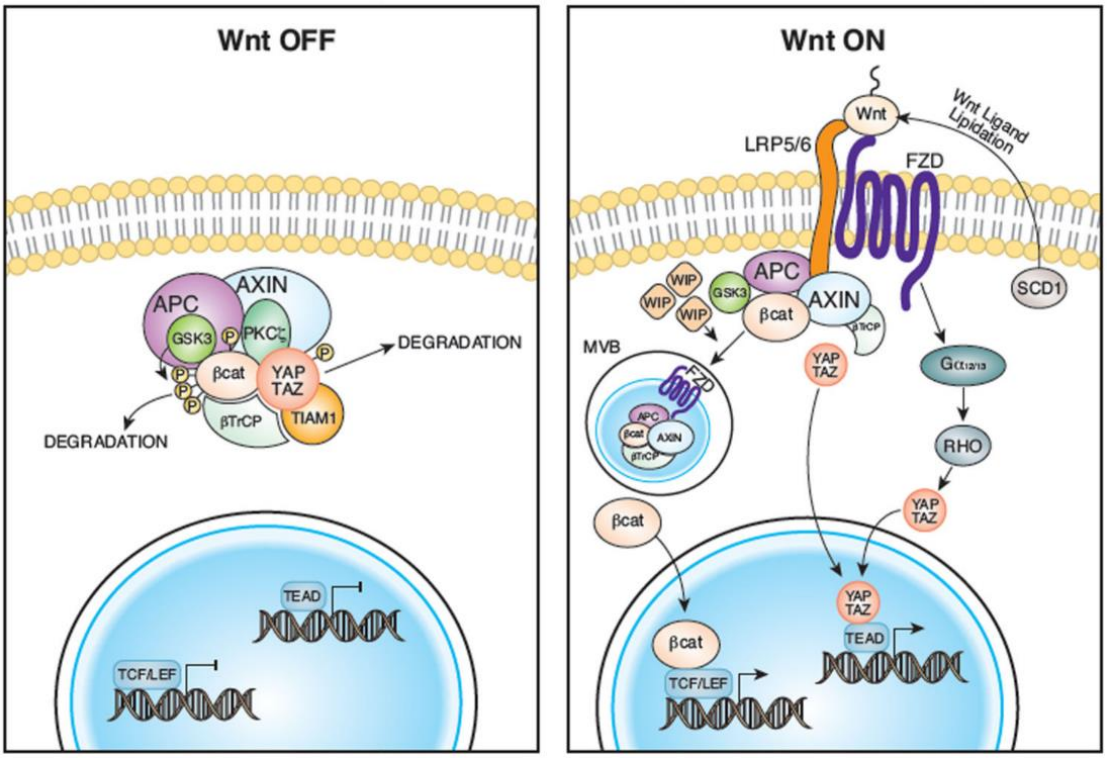

Figure 31: YAP1: the Wnt pathway

YAP/TAZ are components of the Wnt pathway. On the left the pathway is depicted in the "off" state, in which YAP/TAZ are bound in the cytosol. On the right the pathway is shown in "on" state, in which YAP/TAZ can translocate to the nucleus and bind to TEAD. Figure taken from Totaro et al., 2018.

Colon cancer is one of the most pervasive cancers worldwide, which affects both women and men. It is the third most prevalent cancer after breast and lung cancer [96]. Approximately a quarter of colon cancer patients develop metastasis which can occur in the lung, liver, lymph nodes, bone, and brain. Although treatments are available and continuously advancing for metastatic colon cancer, the overall 5-year survival rate is only about 30-40 % [102]. One of the hallmarks of colorectal cancer is the overactivation of Wnt signalling. This contributes to oncogenesis and growth defects with aberrant Wnt activation in approximately 90 % of intestinal tumours [103]. So not only does this pathway contribute to intestinal regeneration, but is also considered a key regulator of early and late and invasive stages of colorectal cancer [9]. With regard to the experiments that were carried out for this thesis only the increase and decrease of YAP1 in the nucleus and cytosol were determined using immunostaining. What is interesting to observe is that in the non-tumorigenic cell line more YAP1 is present in the cytosol as well as the nucleus when compared to the cancer cell line (figure 24). In the HCEC-1CT cell line only the treatment with 25 µM OA led to a decrease in the nucleus and all other treatments were not significant (figure 28). In the HCT 116 cell line with the overall lower

concentration of YAP1 both fatty acids were shown to have an effect on YAP1 translocation. A significant ($p<0,001$) decrease for PA 25 µM, and an increase ($p<0,01$) for OA 25 µM and a significant ($p<0,001$) increase for both 100 µM PA and OA (figure 26). Since YAP1 is involved both in regenerative and cancer promoting processes in the numerous pathways already discussed it is difficult to interpret the available data. To establish a connection between the application of fatty acids and the nuclear translocation of YAP1 it was decided to carry out a further experiment with the HCT 116 cell line under static and under shear stress conditions. To this aim, proteomics will help to determine which changes in protein expression occur due to PA and OA. The analysis for this experiment is in progress however it goes beyond the scope of the present work.

6 Outlook

Through the preceding discussion it has become evident, that the underlying biochemical pathways involved in mechanotransduction and lipid metabolism in the intestine are numerous and highly complex. Beside the results already discussed more experiments are currently being carried out to further elucidate the connection between PA and OA and the mechanosensory apparatus. Proteome analysis of the effect of PA and OA on the HCT 116 cell line in both static and shear stress conditions will be performed to confirm the functional effects of our observations. Rhodamine-labelled PA was used to examine the uptake of PA in both cell lines and will help to clarify the details of the subcellular localization of PA in the different cell lines. Furthermore, experiments investigating the effect of biophysical stimulation through the combination of shear stress with the application of PA and OA in regard to YAP1 translocation in a time dependent manner are currently being carried out. The analysis will be realized after the immunostaining of YAP1. Endpoints in this experiment are 3h, 6h and 24h. As cerulenin had a profound contrasting effect on the different cell lines it would be viable to carry out further experiments to determine combinatory effects of fatty acids and cerulenin in both cell lines. All aforementioned experiments were carried out in 2-D cell models without differentiation, so would be interesting to observe the effects of fatty acid uptake in differentiated cell models displaying villi. Combined with biophysical stimulation the differentiated cell model would even more closely mimic the *in vivo* environment in the intestine.

7 Conclusion

Ongoing research brings forth more knowledge of the interconnectedness of mechanosensitive molecules such as YAP1 and Piezo1 and their roles in health and disease. The results acquired through the experiments carried out in this work are just a tiny fraction of additional knowledge in an ever-expanding field of research. It could be shown that both PA and OA led to a concentration dependent decrease of membrane fluidity in the cancer cell line. Overall, there was no effect on the expression of Piezo1 through the application of PA and OA. However, it was discussed that FASN inhibitor cerulenin had opposing effects on the cell lines, highlighting the fact, that cancer cells and non-tumorigenic cells exhibit different lipid metabolism capabilities leading to differing expression of mechanosensitive Piezo1. Furthermore, there was a very significant increase in actin in the cytoskeleton in both cell lines and for both high and low concentrations of PA and OA. For all treatments and both cell lines higher levels of YAP1 were observed in the nucleus than in the cytosol. Significant reduction of YAP1 could be determined for low concentrations of PA in the nucleus in the HCT 116 cell line and a significant increase of YAP1 for higher concentrations of both PA and OA. Low concentration of OA significantly reduced YAP1 in the nucleus of the HCEC-1CT cell line. However, these treatment dependent changes have to be interpreted in combination with the aforementioned experiments which are still pending, to validate the influence of PA and OA on the mechanosensory apparatus in regard to YAP1. A better understanding of the interrelationship of lipid metabolism and mechanosensory factors, both in healthy and diseased cells have the potential to generate novel methods and refine existing ones to develop applications to maintain and promote intestinal health.

Appendix

Table 3: Substances

Substance	Company	Reference Number	Lot Number
Accutase	Merck	-	3698854
Alexa Fluor™ 568 donkey anti-rabbit IgG (H + L)	Invitrogen	A10042	1964370
BSA FRAC V. Fatty acid, nuc, prot-free	EMD Millipore Corp, USA	M.W. 66000	3563189
Cell mask™ Deep red plasma membrane stain	Invitrogen	C10046	1913941
Cerulenin, Cephalosporium caerulens	EMD Millipore Corp, USA	M.W.223.3	3762630
Cholesterol-Water soluable	Sigma	C4951-30MG	SLBZ
Dimethyl sulfoxide	Carl Roth GmbH + Co. KG, Karlsruhe, GER	A994.1	127253465
Donkey Serum	Sigma Aldrich	D9663-10ML	SLBQ9773
Dulbecco's Modified Eagle Medium	gibco	21063-029	2300364
Dulbecco's Phosphate Buffered Saline	gibco	14190-094	2339098
Fetal calf serum	gibco	10270-106	42GBI93K
Hydrogen peroxide 30%	Carl Roth GmbH + Co. KG, Karlsruhe, GER	8070.2	-
KCl	Roth	67811	479286547
KH_2PO_4	Roth	39041	38908471
Mounting Media	abcam	ab104139	GR3434511-1
MyCoy's 5a Medium	gibco	22330-021	2063605
Na_2HPO_4	Roth	49841	020289971
NaCl	Roth	09662	390289120
Oleic acid	Sigma-Aldrich	O1383-1G	SLCJ8227
Oregon Green®488 phalloidin	Invitrogen	07466	1246105
Palmitic acid	Sigma	P0500-10G	SLCH6263

Palmitic acid – lissamine rhodamine	Avanti	2260669-55-2	810104P-1MG-A-011
PDA 1-Pyrenedecanoic acid	Sigma	82660	BCCC7918
Penicillium streptomycin	Gibco	15140-122	2211097
Piezo1 Polyclonal Antibody	Invitrogen	PA5-106296	VL3141597
Rb m Ab to YAP1	Abcam	Ab 52771	GR3266441-6
Trypsin	gibco	-	461129
WST-1	Rocha	11644807001	45722500

Table 4: Consumables

Consumable	Company	Reference Number	Lot Number
TC Plate 96 Well, Standard d, F	Sarstedt	83.3924	1021821
Neubauer counting chamber	Paul Marienfeld GmbH&Co. KG, GER	0640110	608848
µ-Slide 8 well ibiTreat	ibidi	80826	211129/3
96 Well Optical Btm Plt PolymerBase Black w/Lid	Thermo Scientific	165305	1320775

Table 5: Software

Software	Company
Gen5, 3.08	BioTek Instruments Inc., Winooski, VT, USA
ImageJ, 1.53c	Wayne Rasband, National Institutes of Health, USA
Olympus cellSens Entry, 1.18	Olympus Corporation, Shinjuku, JP
OriginPro®, 2022	OriginLab Corporation,

	Northampton, MA, USA
ZEN 2012 SP5 FP3 (black), 14.0.20.201	Carl Zeiss AG, Oberkochen, GER II
Inkscape 1.2.1	Inkscape Community

Table 6: Devices

Device	Company
CYTATON5762 plate reader	BioTek Instruments Inc., Winooski, VT, USA
Lionheart FX automated microscope	BioTek Instruments Inc., Winooski, VT, USA
Zeiss LSM710 Elyra PS.1	Carl Zeiss AG, Oberkochen, GER

References

[1] Wang, J., Jiang, J., Yang, X., Zhou, G.*, et al.*, Tethering Piezo channels to the actin cytoskeleton for mechanogating via the cadherin-beta-catenin mechanotransduction complex. *Cell Rep* 2022, *38*, 110342.
[2] Ranade, S. S., Syeda, R., Patapoutian, A., Mechanically Activated Ion Channels. *Neuron* 2015, *87*, 1162-1179.
[3] Tarbell, J. M., Pahakis, M. Y., Mechanotransduction and the glycocalyx. *J Intern Med* 2006, *259*, 339-350.
[4] De Felice, D., Alaimo, A., Mechanosensitive Piezo Channels in Cancer: Focus on altered Calcium Signaling in Cancer Cells and in Tumor Progression. *Cancers (Basel)* 2020, *12*.
[5] Ando, J., Yamamoto, K., Hemodynamic Forces, Endothelial Mechanotransduction, and Vascular Diseases. *Magn Reson Med Sci* 2022, *21*, 258-266.
[6] Perez-Gonzalez, C., Ceada, G., Matejcic, M., Trepat, X., Digesting the mechanobiology of the intestinal epithelium. *Curr Opin Genet Dev* 2022, *72*, 82-90.
[7] van der Flier, L. G., Clevers, H., Stem cells, self-renewal, and differentiation in the intestinal epithelium. *Annu Rev Physiol* 2009, *71*, 241-260.
[8] Shoshkes-Carmel, M., Wang, Y. J., Wangensteen, K. J., Toth, B.*, et al.*, Subepithelial telocytes are an important source of Wnts that supports intestinal crypts. *Nature* 2018, *557*, 242-246.
[9] Basu, S., Haase, G., Ben-Ze'ev, A., Wnt signaling in cancer stem cells and colon cancer metastasis. *F1000Res* 2016, *5*.
[10] Anishkin, A., Loukin, S. H., Teng, J., Kung, C., Feeling the hidden mechanical forces in lipid bilayer is an original sense. *Proc Natl Acad Sci U S A* 2014, *111*, 7898-7905.
[11] Douguet, D., Honore, E., Mammalian Mechanoelectrical Transduction: Structure and Function of Force-Gated Ion Channels. *Cell* 2019, *179*, 340-354.
[12] Teng, J., Loukin, S., Anishkin, A., Kung, C., The force-from-lipid (FFL) principle of mechanosensitivity, at large and in elements. *Pflugers Arch* 2015, *467*, 27-37.
[13] Cox, C. D., Bavi, N., Martinac, B., Biophysical Principles of Ion-Channel-Mediated Mechanosensory Transduction. *Cell Rep* 2019, *29*, 1-12.
[14] Beech, D. J., Lichtenstein, L., RNA and the PIEZO force sensor. *Cell Res* 2020, *30*, 829-830.
[15] Alcaino, C., Farrugia, G., Beyder, A., Mechanosensitive Piezo Channels in the Gastrointestinal Tract. *Curr Top Membr* 2017, *79*, 219-244.
[16] Piccolo, S., Dupont, S., Cordenonsi, M., The biology of YAP/TAZ: hippo signaling and beyond. *Physiol Rev* 2014, *94*, 1287-1312.
[17] Koo, J. H., Guan, K. L., Interplay between YAP/TAZ and Metabolism. *Cell Metab* 2018, *28*, 196-206.
[18] Mohri, Z., Del Rio Hernandez, A., Krams, R., The emerging role of YAP/TAZ in mechanotransduction. *J Thorac Dis* 2017, *9*, E507-E509.
[19] Waters, C. M., Roan, E., Navajas, D., Mechanobiology in lung epithelial cells: measurements, perturbations, and responses. *Compr Physiol* 2012, *2*, 1-29.
[20] Brusatin, G., Panciera, T., Gandin, A., Citron, A., Piccolo, S., Biomaterials and engineered microenvironments to control YAP/TAZ-dependent cell behaviour. *Nat Mater* 2018, *17*, 1063-1075.
[21] Gregor, T., Beyond D'Arcy Thompson: Future challenges for quantitative biology. *Mech Dev* 2017, *145*, 10-12.
[22] Chatterjee, S., Fisher, A. B., Mechanotransduction in the endothelium: role of membrane proteins and reactive oxygen species in sensing, transduction, and transmission of the signal with altered blood flow. *Antioxid Redox Signal* 2014, *20*, 899-913.

[23] Marcantonio, E. E., Hynes, R. O., Antibodies to the conserved cytoplasmic domain of the integrin beta 1 subunit react with proteins in vertebrates, invertebrates, and fungi. *J Cell Biol* 1988, *106*, 1765-1772.
[24] Del Favero, G., Kraegeloh, A., Integrating Biophysics in Toxicology. *Cells* 2020, *9*.
[25] Leckband, D. E., le Duc, Q., Wang, N., de Rooij, J., Mechanotransduction at cadherin-mediated adhesions. *Curr Opin Cell Biol* 2011, *23*, 523-530.
[26] Stutchbury, B., Atherton, P., Tsang, R., Wang, D. Y., Ballestrem, C., Distinct focal adhesion protein modules control different aspects of mechanotransduction. *J Cell Sci* 2017, *130*, 1612-1624.
[27] Singer, S. J., Nicolson, G. L., The fluid mosaic model of the structure of cell membranes. *Science* 1972, *175*, 720-731.
[28] Nicolson, G. L., Ferreira de Mattos, G., A Brief Introduction to Some Aspects of the Fluid-Mosaic Model of Cell Membrane Structure and Its Importance in Membrane Lipid Replacement. *Membranes (Basel)* 2021, *11*.
[29] Israelachvili, J. N., Marcelja, S., Horn, R. G., Physical principles of membrane organization. *Q Rev Biophys* 1980, *13*, 121-200.
[30] Ikonen, E., Cellular cholesterol trafficking and compartmentalization. *Nat Rev Mol Cell Biol* 2008, *9*, 125-138.
[31] Goni, F. M., The basic structure and dynamics of cell membranes: an update of the Singer-Nicolson model. *Biochim Biophys Acta* 2014, *1838*, 1467-1476.
[32] Gruner, S. M., Intrinsic curvature hypothesis for biomembrane lipid composition: a role for nonbilayer lipids. *Proc Natl Acad Sci U S A* 1985, *82*, 3665-3669.
[33] Singer, S. J., The molecular organization of membranes. *Annu Rev Biochem* 1974, *43*, 805-833.
[34] Moroni, M., Servin-Vences, M. R., Fleischer, R., Sanchez-Carranza, O., Lewin, G. R., Voltage gating of mechanosensitive PIEZO channels. *Nat Commun* 2018, *9*, 1096.
[35] Douguet, D., Patel, A., Xu, A., Vanhoutte, P. M., Honore, E., Piezo Ion Channels in Cardiovascular Mechanobiology. *Trends Pharmacol Sci* 2019, *40*, 956-970.
[36] Alcaino, C., Knutson, K. R., Treichel, A. J., Yildiz, G.*, et al.*, A population of gut epithelial enterochromaffin cells is mechanosensitive and requires Piezo2 to convert force into serotonin release. *Proc Natl Acad Sci U S A* 2018, *115*, E7632-E7641.
[37] Chesler, A. T., Szczot, M., Bharucha-Goebel, D., Ceko, M.*, et al.*, The Role of PIEZO2 in Human Mechanosensation. *N Engl J Med* 2016, *375*, 1355-1364.
[38] Della Pietra, A., Mikhailov, N., Giniatullin, R., The Emerging Role of Mechanosensitive Piezo Channels in Migraine Pain. *Int J Mol Sci* 2020, *21*.
[39] Linan-Rico, A., Ochoa-Cortes, F., Beyder, A., Soghomonyan, S.*, et al.*, Mechanosensory Signaling in Enterochromaffin Cells and 5-HT Release: Potential Implications for Gut Inflammation. *Front Neurosci* 2016, *10*, 564.
[40] Wang, X., Cheng, G., Miao, Y., Qiu, F.*, et al.*, Piezo type mechanosensitive ion channel component 1 facilitates gastric cancer omentum metastasis. *J Cell Mol Med* 2021, *25*, 2238-2253.
[41] Bai, T., Li, Y., Xia, J., Jiang, Y.*, et al.*, Piezo2: A Candidate Biomarker for Visceral Hypersensitivity in Irritable Bowel Syndrome? *J Neurogastroenterol Motil* 2017, *23*, 453-463.
[42] Zhao, Q., Zhou, H., Chi, S., Wang, Y.*, et al.*, Structure and mechanogating mechanism of the Piezo1 channel. *Nature* 2018, *554*, 487-492.
[43] Zhao, Q., Wu, K., Geng, J., Chi, S.*, et al.*, Ion Permeation and Mechanotransduction Mechanisms of Mechanosensitive Piezo Channels. *Neuron* 2016, *89*, 1248-1263.
[44] Wang, F., Knutson, K., Alcaino, C., Linden, D. R.*, et al.*, Mechanosensitive ion channel Piezo2 is important for enterochromaffin cell response to mechanical forces. *J Physiol* 2017, *595*, 79-91.
[45] Fang, X. Z., Zhou, T., Xu, J. Q., Wang, Y. X.*, et al.*, Structure, kinetic properties and biological function of mechanosensitive Piezo channels. *Cell Biosci* 2021, *11*, 13.
[46] Wang, L., Zhou, H., Zhang, M., Liu, W.*, et al.*, Structure and mechanogating of the mammalian tactile channel PIEZO2. *Nature* 2019, *573*, 225-229.
[47] Gefen, A., Weihs, D., Mechanical cytoprotection: A review of cytoskeleton-protection approaches for cells. *J Biomech* 2016, *49*, 1321-1329.

[48] Romero, S., Le Clainche, C., Gautreau, A. M., Actin polymerization downstream of integrins: signaling pathways and mechanotransduction. *Biochem J* 2020, *477*, 1-21.
[49] Pollard, T. D., Cooper, J. A., Actin, a central player in cell shape and movement. *Science* 2009, *326*, 1208-1212.
[50] Chambliss, A. B., Khatau, S. B., Erdenberger, N., Robinson, D. K.*, et al.*, The LINC-anchored actin cap connects the extracellular milieu to the nucleus for ultrafast mechanotransduction. *Sci Rep* 2013, *3*, 1087.
[51] Gourlay, C. W., Ayscough, K. R., The actin cytoskeleton in ageing and apoptosis. *FEMS Yeast Res* 2005, *5*, 1193-1198.
[52] Aramaki, S., Mayanagi, K., Jin, M., Aoyama, K., Yasunaga, T., Filopodia formation by crosslinking of F-actin with fascin in two different binding manners. *Cytoskeleton (Hoboken)* 2016, *73*, 365-374.
[53] Gal, N., Weihs, D., Intracellular mechanics and activity of breast cancer cells correlate with metastatic potential. *Cell Biochem Biophys* 2012, *63*, 199-209.
[54] Li, Q. S., Lee, G. Y., Ong, C. N., Lim, C. T., AFM indentation study of breast cancer cells. *Biochem Biophys Res Commun* 2008, *374*, 609-613.
[55] Reddy, P., Deguchi, M., Cheng, Y., Hsueh, A. J., Actin cytoskeleton regulates Hippo signaling. *PLoS One* 2013, *8*, e73763.
[56] Totaro, A., Panciera, T., Piccolo, S., YAP/TAZ upstream signals and downstream responses. *Nat Cell Biol* 2018, *20*, 888-899.
[57] Elosegui-Artola, A., Andreu, I., Beedle, A. E. M., Lezamiz, A.*, et al.*, Force Triggers YAP Nuclear Entry by Regulating Transport across Nuclear Pores. *Cell* 2017, *171*, 1397-1410 e1314.
[58] Codelia, V. A., Sun, G., Irvine, K. D., Regulation of YAP by mechanical strain through Jnk and Hippo signaling. *Curr Biol* 2014, *24*, 2012-2017.
[59] Bertini, E., Oka, T., Sudol, M., Strano, S., Blandino, G., YAP: at the crossroad between transformation and tumor suppression. *Cell Cycle* 2009, *8*, 49-57.
[60] Anbanandam, A., Albarado, D. C., Nguyen, C. T., Halder, G.*, et al.*, Insights into transcription enhancer factor 1 (TEF-1) activity from the solution structure of the TEA domain. *Proc Natl Acad Sci U S A* 2006, *103*, 17225-17230.
[61] Santinon, G., Pocaterra, A., Dupont, S., Control of YAP/TAZ Activity by Metabolic and Nutrient-Sensing Pathways. *Trends Cell Biol* 2016, *26*, 289-299.
[62] Wang, Z., Wu, Y., Wang, H., Zhang, Y.*, et al.*, Interplay of mevalonate and Hippo pathways regulates RHAMM transcription via YAP to modulate breast cancer cell motility. *Proc Natl Acad Sci U S A* 2014, *111*, E89-98.
[63] Enzo, E., Santinon, G., Pocaterra, A., Aragona, M.*, et al.*, Aerobic glycolysis tunes YAP/TAZ transcriptional activity. *EMBO J* 2015, *34*, 1349-1370.
[64] Wolfrum, C., Asilmaz, E., Luca, E., Friedman, J. M., Stoffel, M., Foxa2 regulates lipid metabolism and ketogenesis in the liver during fasting and in diabetes. *Nature* 2004, *432*, 1027-1032.
[65] Wang, D. D., Li, Y., Chiuve, S. E., Stampfer, M. J.*, et al.*, Association of Specific Dietary Fats With Total and Cause-Specific Mortality. *JAMA Intern Med* 2016, *176*, 1134-1145.
[66] Carta, G., Murru, E., Banni, S., Manca, C., Palmitic Acid: Physiological Role, Metabolism and Nutritional Implications. *Front Physiol* 2017, *8*, 902.
[67] Carta, G., Murru, E., Lisai, S., Sirigu, A.*, et al.*, Dietary triacylglycerols with palmitic acid in the sn-2 position modulate levels of N-acylethanolamides in rat tissues. *PLoS One* 2015, *10*, e0120424.
[68] Song, X., Huang, Y., Neuhouser, M. L., Tinker, L. F.*, et al.*, Dietary long-chain fatty acids and carbohydrate biomarker evaluation in a controlled feeding study in participants from the Women's Health Initiative cohort. *Am J Clin Nutr* 2017, *105*, 1272-1282.
[69] Wilke, M. S., French, M. A., Goh, Y. K., Ryan, E. A.*, et al.*, Synthesis of specific fatty acids contributes to VLDL-triacylglycerol composition in humans with and without type 2 diabetes. *Diabetologia* 2009, *52*, 1628-1637.
[70] Pascual, G., Avgustinova, A., Mejetta, S., Martin, M.*, et al.*, Targeting metastasis-initiating cells through the fatty acid receptor CD36. *Nature* 2017, *541*, 41-45.

[71] Kwan, H. Y., Liu, B., Huang, C., Fatima, S*., et al.*, Signal transducer and activator of transcription-3 drives the high-fat diet-associated prostate cancer growth. *Cell Death Dis* 2019, *10*, 637.
[72] Wang, Q., Liu, R., Chang, M., Zhang, H*., et al.*, Dietary oleic acid supplementation and blood inflammatory markers: a systematic review and meta-analysis of randomized controlled trials. *Crit Rev Food Sci Nutr* 2022, *62*, 2508-2525.
[73] Llor, X., Pons, E., Roca, A., Alvarez, M*., et al.*, The effects of fish oil, olive oil, oleic acid and linoleic acid on colorectal neoplastic processes. *Clin Nutr* 2003, *22*, 71-79.
[74] Menendez, J. A., Lupu, R., Mediterranean dietary traditions for the molecular treatment of human cancer: anti-oncogenic actions of the main olive oil's monounsaturated fatty acid oleic acid (18:1n-9). *Curr Pharm Biotechnol* 2006, *7*, 495-502.
[75] Funabashi, H., Kawaguchi, A., Tomoda, H., Omura, S*., et al.*, Binding site of cerulenin in fatty acid synthetase. *J Biochem* 1989, *105*, 751-755.
[76] Kawaguchi, A., Tomoda, H., Okuda, S., Awaya, J., Omura, S., Cerulenin resistance in a cerulenin-producing fungus. Isolation of cerulenin insensitive fatty acid synthetase. *Arch Biochem Biophys* 1979, *197*, 30-35.
[77] Straub, S. G., Yajima, H., Komatsu, M., Aizawa, T., Sharp, G. W., The effects of cerulenin, an inhibitor of protein acylation, on the two phases of glucose-stimulated insulin secretion. *Diabetes* 2002, *51 Suppl 1*, S91-95.
[78] Fatima, S., Hu, X., Huang, C., Zhang, W*., et al.*, High-fat diet feeding and palmitic acid increase CRC growth in beta2AR-dependent manner. *Cell Death Dis* 2019, *10*, 711.
[79] Roig, A. I., Eskiocak, U., Hight, S. K., Kim, S. B*., et al.*, Immortalized epithelial cells derived from human colon biopsies express stem cell markers and differentiate in vitro. *Gastroenterology* 2010, *138*, 1012-1021 e1011-1015.
[80] Del Favero, G., Zaharescu, R., Marko, D., Functional impairment triggered by altertoxin II (ATXII) in intestinal cells in vitro: cross-talk between cytotoxicity and mechanotransduction. *Arch Toxicol* 2018, *92*, 3535-3547.
[81] Zunszain, P. A., Ghuman, J., Komatsu, T., Tsuchida, E., Curry, S., Crystal structural analysis of human serum albumin complexed with hemin and fatty acid. *BMC Struct Biol* 2003, *3*, 6.
[82] Li, S., Sun, C., Gu, Y., Gao, X*., et al.*, Mutation of IDH1 aggravates the fatty acidinduced oxidative stress in HCT116 cells by affecting the mitochondrial respiratory chain. *Mol Med Rep* 2019, *19*, 2509-2518.
[83] Peskin, A. V., Winterbourn, C. C., Assay of superoxide dismutase activity in a plate assay using WST-1. *Free Radic Biol Med* 2017, *103*, 188-191.
[84] Peskin, A. V., Winterbourn, C. C., A microtiter plate assay for superoxide dismutase using a water-soluble tetrazolium salt (WST-1). *Clin Chim Acta* 2000, *293*, 157-166.
[85] Tan, A. S., Berridge, M. V., Superoxide produced by activated neutrophils efficiently reduces the tetrazolium salt, WST-1 to produce a soluble formazan: a simple colorimetric assay for measuring respiratory burst activation and for screening anti-inflammatory agents. *J Immunol Methods* 2000, *238*, 59-68.
[86] Zhang, X., Hurng, J., Rateri, D. L., Daugherty, A*., et al.*, Membrane cholesterol modulates the fluid shear stress response of polymorphonuclear leukocytes via its effects on membrane fluidity. *Am J Physiol Cell Physiol* 2011, *301*, C451-460.
[87] Del Favero, G., Mayer, R. M., Dellafiora, L., Janker, L*., et al.*, Structural Similarity with Cholesterol Reveals Crucial Insights into Mechanisms Sustaining the Immunomodulatory Activity of the Mycotoxin Alternariol. *Cells* 2020, *9*.
[88] Romero, L. O., Massey, A. E., Mata-Daboin, A. D., Sierra-Valdez, F. J*., et al.*, Dietary fatty acids fine-tune Piezo1 mechanical response. *Nat Commun* 2019, *10*, 1200.
[89] Sok, M., Sentjurc, M., Schara, M., Stare, J., Rott, T., Cell membrane fluidity and prognosis of lung cancer. *Ann Thorac Surg* 2002, *73*, 1567-1571.
[90] Shinitzky, M., Skornick, Y., Gorelik, E., Sindelar, W., Regulation of membrane function by lipids; implications for tumor development. *Prog Clin Biol Res* 1983, *132B*, 425-433.

[91] Rebhahn, V. I. C., Kiss, E., Marko, D., Del Favero, G., Foodborne compounds that alter plasma membrane architecture can modify the response of intestinal cells to shear stress in vitro. *Toxicol Appl Pharmacol* 2022, *446*, 116034.
[92] Head, B. P., Patel, H. H., Insel, P. A., Interaction of membrane/lipid rafts with the cytoskeleton: impact on signaling and function: membrane/lipid rafts, mediators of cytoskeletal arrangement and cell signaling. *Biochim Biophys Acta* 2014, *1838*, 532-545.
[93] Smith, S., The animal fatty acid synthase: one gene, one polypeptide, seven enzymes. *FASEB J* 1994, *8*, 1248-1259.
[94] Chirala, S. S., Jayakumar, A., Gu, Z. W., Wakil, S. J., Human fatty acid synthase: role of interdomain in the formation of catalytically active synthase dimer. *Proc Natl Acad Sci U S A* 2001, *98*, 3104-3108.
[95] Schroeder, B., Vander Steen, T., Espinoza, I., Venkatapoorna, C. M. K.*, et al.*, Fatty acid synthase (FASN) regulates the mitochondrial priming of cancer cells. *Cell Death Dis* 2021, *12*, 977.
[96] Zhou, M., Liu, X., Li, Z., Huang, Q.*, et al.*, Caspase-3 regulates the migration, invasion and metastasis of colon cancer cells. *Int J Cancer* 2018, *143*, 921-930.
[97] Shiragami, R., Murata, S., Kosugi, C., Tezuka, T.*, et al.*, Enhanced antitumor activity of cerulenin combined with oxaliplatin in human colon cancer cells. *Int J Oncol* 2013, *43*, 431-438.
[98] Pizer, E. S., Thupari, J., Han, W. F., Pinn, M. L.*, et al.*, Malonyl-coenzyme-A is a potential mediator of cytotoxicity induced by fatty-acid synthase inhibition in human breast cancer cells and xenografts. *Cancer Res* 2000, *60*, 213-218.
[99] Pinto, D., Gregorieff, A., Begthel, H., Clevers, H., Canonical Wnt signals are essential for homeostasis of the intestinal epithelium. *Genes Dev* 2003, *17*, 1709-1713.
[100] Potten, C. S., Grant, H. K., The relationship between ionizing radiation-induced apoptosis and stem cells in the small and large intestine. *Br J Cancer* 1998, *78*, 993-1003.
[101] Guillermin, O., Angelis, N., Sidor, C. M., Ridgway, R.*, et al.*, Wnt and Src signals converge on YAP-TEAD to drive intestinal regeneration. *EMBO J* 2021, *40*, e105770.
[102] Bartlett, D. L., Chu, E., Can metastatic colorectal cancer be cured? *Oncology (Williston Park)* 2012, *26*, 266-275.
[103] Clevers, H., Wnt/beta-catenin signaling in development and disease. *Cell* 2006, *127*, 469-480.